Pair structure of the hard-sphere Yukawa fluid: An improved analytic method versus simulations, Rogers-Young scheme, and experiment

Marco Heinen, Peter Holmqvist, Adolfo J. Banchio, and Gerhard Nägele

Additional information on J. Chem. Phys.

Pair structure of the hard-sphere Yukawa fluid: An improved analytic method versus simulations, Rogers-Young scheme, and experiment

Marco Heinen,[1,a)] Peter Holmqvist,[1] Adolfo J. Banchio,[2] and Gerhard Nägele[1]

[1]*Institut für Festkörperforschung, Teilinstitut Weiche Materie, Forschungszentrum Jülich, D-52425 Jülich, Germany*
[2]*FaMAF, Universidad Nacional de Córdoba, IFEG-CONICET, Ciudad Universitaria, 5000 Córdoba, Argentina*

We present a comprehensive study of the equilibrium pair structure in fluids of nonoverlapping spheres interacting by a repulsive Yukawa-like pair potential, with special focus on suspensions of charged colloidal particles. The accuracy of several integral equation schemes for the static structure factor, $S(q)$, and radial distribution function, $g(r)$, is investigated in comparison to computer simulation results and static light scattering data on charge-stabilized silica spheres. In particular, we show that an improved version of the so-called penetrating-background corrected rescaled mean spherical approximation (PB-RMSA) by Snook and Hayter [Langmuir **8**, 2880 (1992)], referred to as the modified PB-RMSA (MPB-RMSA), gives pair structure functions which are in general in very good agreement with Monte Carlo simulations and results from the accurate but nonanalytical and therefore computationally more expensive Rogers-Young integral equation scheme. The MPB-RMSA preserves the analytic simplicity of the standard rescaled mean spherical (RMSA) solution. The combination of high accuracy and fast evaluation makes the MPB-RMSA ideally suited for extensive parameter scans and experimental data evaluation, and for providing the static input to dynamic theories. We discuss the results of extensive parameter scans probing the concentration scaling of the pair structure of strongly correlated Yukawa particles, and we determine the liquid-solid coexistence line using the Hansen-Verlet freezing rule. © *2011 American Institute of Physics.* [doi:10.1063/1.3524309]

I. INTRODUCTION

The model system of hard spheres with Yukawa-type repulsive pair interaction, commonly referred to as the hard-sphere Yukawa (HSY) fluid, has been extensively used as a reference system for a large variety of atomic systems including plasmas and liquid metals,[1–3] and alloys.[4,5] In the HSY model, the pair potential is taken to be

$$\beta u(x) = \begin{cases} \infty, & x = r/\sigma < 1, \\ \gamma \dfrac{e^{-kx}}{x}, & x > 1, \end{cases} \tag{1}$$

where $\sigma = 2a$ is the hard-core diameter, r is the center-to-center distance between two particles, and $\beta = 1/(k_B T)$ with absolute temperature T and Boltzmann's constant k_B. The dimensionless coupling parameter γ and the screening parameter $k \geq 0$ characterize, respectively, the strength and range of the Yukawa potential tail. For the important class of repelling Yukawa particles exclusively considered in this paper, γ is nonnegative. Changing k allows for the variation of the pair potential from pure hard-core interactions to a Coulomb potential, the latter describing a one-component plasma-like behavior. This versatility is the reason for the prominent role of the HSY model in liquid state theory.

In addition to atomic systems, the HSY model has found its most widespread application in the study of the equilib-

rium structure, dynamics and phase behavior of macromolecular systems, including suspensions of large charge-stabilized colloidal spheres,[6–17] and solutions of globular charged proteins,[18,19] micelles[20,21] and short DNA fragments.[22] In the standard Derjaguin-Landau-Verwey-Overbeek (DLVO) theory of colloidal charge stabilization,[23] the screened Coulomb repulsion of two charged colloidal particles (macroions) caused by the overlap of their diffuse microionic clouds, is represented by Eq. (1) with the coupling parameter determined by

$$\gamma = \frac{L_B}{\sigma} \left(\frac{e^{k/2}}{1 + k/2} \right)^2 Z^2. \tag{2}$$

Here, $L_B = \beta e^2 / \epsilon$ is the solvent-characteristic Bjerrum length in Gaussian units, ϵ is the solvent dielectric constant, and Z is the effective macroion charge number in units of the proton elementary charge e. For monovalent counterions released from the macroion surfaces, and added 1-1 electrolyte, the screening parameter is determined by

$$k^2 = \frac{L_B/\sigma}{1 - \phi} \left(24\phi |Z| + 8\pi n_s \sigma^3 \right), \tag{3}$$

where n and $\phi = (\pi/6)n\sigma^3$ are, respectively, the colloidal number concentration and volume fraction, and $2n_s$ is the concentration of added monovalent salt ions. The electric DLVO potential given by Eqs. (1)–(3) has been derived, as the potential of mean force in the limit $\phi \to 0$, on the basis of the

---

a)Electronic mail: m.heinen@fz-juelich.de.

linearized Poisson-Boltzmann theory[23] and the linear mean-spherical approximation (MSA) for a highly asymmetric ionic mixture,[24–26] on assuming point-like (monovalent) counter- and coions (microions) and $L_B Z^2/\sigma \ll 1$. For more strongly charged macroions, the DLVO potential can be still used, but Z should be interpreted then as an effective macroion charge number smaller than the bare one, since it includes a correction for the fraction of surface-condensed counterions. The effective macroion charge Z in relation to the bare one can be estimated using simplifying mean-field-type cell model[27, 28] or selfconsistent jellium model calculations,[22, 29, 30] and non-mean field extensions describing macroion overcharging and ion-pairing effects in multivalent electrolytes[31]. Due to the approximative nature of all these calculations, different values for Z are obtained.

The factor $1/(1 - \phi)$ in Eq. (3), relevant for larger colloid concentrations, has been discussed in Refs. 32 and 33. It corrects for the free volume accessible to the microions, which can not penetrate the colloidal cores.

In the present paper, we are not concerned with the on-going discussion on how the effective charge is quantitatively related to the bare one, with the latter commonly defined on a more fundamental level where macroions and microions are treated on equal footing as (nonpolarizable) charged hard spheres immersed in a structureless fluid. Nor will we be concerned here with nonpairwise additivity effects appearing as macroion screening which can be accounted for approximately by a concentration-dependent cutoff of the electric DLVO potential.[34] It has been shown in many applications that the static structure factor, $S(q)$, of a large variety of charge-stabilized colloids can be consistently described on the basis of the electric DLVO pair potential, with the effective charge Z as the basic fitting parameter.

In applying the HSY model to macromolecular ionic systems, one assumes that the influence of attractive dispersion forces on the macroions is negligible relative to the electric repulsion. This assumption is justified when the macromolecular particles are strongly charged and when the electrostatic screening described by k is sufficiently small, like in low-salinity systems, or when the dielectric mismatch of particles and solvent is small.

The hard-core part of the HSY potential is irrelevant for the most important class of charged colloid systems where contact configurations are extremely unlikely. These systems have in common a practically zero contact value, $g(r = \sigma^+) \approx 0$, of the radial distribution function (rdf), with $g(r)$ quantifying the conditional probability in an isotropic fluid of finding a particle a distance r from a given one. All these systems share the geometrical mean particle distance, $\tilde{d} = n^{-1/3}$, as the natural characteristic length unit. In terms of this length unit,

$$\beta u(\tilde{x} > \sigma/\tilde{d}) = \tilde{\gamma} \exp\{-\tilde{k}\tilde{x}\} \qquad (4)$$

with $\tilde{x} = r/\tilde{d}$ and reduced potential parameters $\tilde{\gamma} = \gamma\sigma/\tilde{d}$ and $\tilde{k} = k\tilde{d}/\sigma$. Since the hard-core overlap region, $\tilde{x} < \sigma/\tilde{d}$, is of no physical relevance for these systems, the Yukawa potential in Eq. (4) can be extrapolated down to $\tilde{x} = 0$ without affecting the microstructure. In the same length unit, the

Ornstein-Zernike equation[3] is expressed as

$$h(\tilde{x}) = c(\tilde{x}) + \int d\tilde{\mathbf{x}}' \, h(\tilde{x}') c(|\tilde{\mathbf{x}} - \tilde{\mathbf{x}}'|), \qquad (5)$$

where $c(r)$ and $h(r) = g(r) - 1$ are, respectively, the direct and total correlation functions related to the radial distribution function. We see here that the class of HSY systems of zero contact value are fully characterized by the two dimensionless parameters $\tilde{\gamma}$ and $\tilde{k}$. On the other hand, four dimensionless parameter groups which are experimentally controllable to some extent, namely $\{L_B/\sigma, Z, n_s\sigma^3, \phi\}$, enter into the DLVO potential. Thus, different combinations of these four parameters sharing the same $(\tilde{\gamma}, \tilde{k})$ values have identical functions $S(q)$ and $g(r)$, for the wavenumber q and the pair distance r expressed in units of $\tilde{d}$, and under the proviso that they fall into the $g(\sigma^+) \approx 0$ class. The phase diagram of these (effectively point-like) Yukawa particles of hard-core interactions masked by the Yukawa tail is quite simple, with a single fluid phase that can freeze into a fcc or bcc solid. The diagram has a single triple point but no critical point since the potential is purely repulsive.[35–38] A recent discussion of the critical point in hard-sphere plus attractive Yukawa-tail fluids is given in Ref. 39. The extended phase diagram including HSY systems with $g(\sigma^+) > 0$, i.e., systems where the rdf is discontinuous at contact distance, is somewhat more complicated, showing an additional fluid-fcc-bcc triple point.[34, 40] Systems where the hard core matters are characterized by three dimensionless parameters, namely by (γ, k, ϕ), with σ as the natural length unit. Systems of equal (γ, k, ϕ) share the same $S(q)$ expressed as a function of $q\sigma$.

An important feature of the HSY model is that, in conjunction with the MSA closure relation,[3]

$$c(r > \sigma) = -\beta u(r), \qquad (6)$$

for the direct correlation function $c(r)$, and the exact zero-overlap condition $g(r < \sigma) = 0$, an essentially analytic solution of the Ornstein-Zernike equation is obtained for $S(q)$. This is a desirable feature since $S(q)$ is the key quantity determined in static scattering experiments. The MSA solution was first derived for general k by Waisman,[41] and in the limit of no screening ($k = 0$) also by Palmer and Weeks.[1] The original MSA solution by Waisman includes a rather complex set of algebraic equations from which the unique, physically allowed structure factor must be deduced. The MSA solution was further simplified by Blum and Hoye,[42] and Cummings and Smith.[43, 44] A particularly simple form of the MSA solution was obtained more recently by Ginoza[45] (see also Ref. 5), invoking a simple quartic algebraic equation from which the physical root is straightforwardly deduced.

While the MSA solution applies well to dense suspensions of more weakly charged macroions such as charged micelles,[20, 21] it is known to fail for the important case of strongly charged colloidal particles under low-volume fraction conditions such as suspensions of polystyrene spheres in water. Due to the nonexact treatment of shorter-ranged correlations in the MSA closure relation which is only asymptotically exact, nonphysical negative values of $g(r)$ are predicted near the contact distance σ of two particles for low concentrations and strong repulsion. This undesired feature is absent in the case of an attractive Yukawa tail. As shown by Hansen and

Hayter,[46] this severe deficiency of the MSA can be remedied by increasing the hard-sphere diameter, σ, of the HSY spheres at fixed particle concentration to a larger value $\sigma' > \sigma$, without altering the form of the Yukawa-tail of the pair potential. The rescaled effective diameter σ' is determined from the physical constraint that the $g(r)$ in these systems must be continuous, i.e., from requiring the Gillan condition that $g(r = \sigma'^+; \phi') = 0$ (Ref. [47]) where $\phi' = \phi(\sigma'/\sigma)^3 > \phi$ is the rescaled volume fraction. The underlying physical picture is that in strongly repulsive systems, where the finite particle size plays no physical role, a family of systems with same soft Yukawa tail but different hard-sphere diameters should share the same $g(r)$, provided all diameters are smaller than σ'. Since the MSA is reasonably accurate at larger volume fractions without featuring negative values for the rdf, $g_{\text{RMSA}}(r) = g_{\text{MSA}}(r; \sigma', \phi')$ becomes a reasonably good approximation for the rdf characterizing this family of systems. The diameter-rescaled MSA is referred to as the RMSA.[46]

The RMSA scheme of Hansen and Hayter preserves the analyticity of the original MSA solution without sharing its deficiency at low ϕ and for strong Yukawa tail repulsion. This is the reason why the RMSA is widely used to this date as an efficient tool for calculating the pair structure, for fitting scattering data (see, e.g., its implementation in Ref. [48]), and for delivering the static input to theoretical schemes predicting equilibrium and nonequilibrium colloidal transport properties and phase boundaries.[6,8,13,16,49,50] Note here that an extension of the rescaled MSA to mixtures of hard-sphere Yukawa particles of differing diameters and Yukawa tails has been discussed by Ruiz-Estrada et al.[26]

The RMSA constitutes a considerable improvement over the MSA. However, comparisons with computer simulations and results from the highly accurate but numerically more expensive Rogers-Young (RY) integral equation scheme,[51] reveal that the RMSA typically tends to underestimate the local ordering of strongly repulsive particles. This is most strongly noticed in the underestimated principal peak values of $S(q)$ and $g(r)$, and in the overestimation of the reduced osmotic compressibility $\lim_{q \to 0} S(q)$. Therefore, it is desirable to find an improved scheme that takes advantage of the analytic simplicity of the RMSA solution. Using a simple argument related to the uniform neutralizing charge background of the one-component plasma model (OCP), Snook and Hayter[52] provided such an improved scheme. They have demonstrated this in comparison with a number of simulation results for $g(r)$ (see also Ref. [53]). Unfortunately, in spite of its simplicity and usefulness, their so-called penetrating-background (PB) corrected RMSA scheme (PB-RMSA, for short) has remained largely unnoticed and unused both in the colloid and liquid metal communities.

In Sec. II, we summarize the essentials of Snook and Hayter's PB-RMSA scheme, and we improve its accuracy by a straightforward modification of the underlying screening parameter. We refer to our modified scheme as the MPB-RMSA method. The MPB-RMSA further improves the general agreement with simulation data for $S(q)$ and $g(r)$, and for the osmotic compressibility in particular. The algorithm of the MPB-RMSA is summarized in the Appendix, for readers interested in its implementation.

In Sec. III, the good performance of the fast MPB-RMSA is assessed over the full HSY fluid-phase space, in comparison with a large number of RY and Monte Carlo (MC) simulation results, and with predictions of the pair structure by the less accurate hypernetted-chain (HNC) and RMSA integral equation schemes. For strongly correlated particles of high surface charge under low-salt conditions, the accuracy of the predicted $S(q)$ and $g(r)$ is unprecedented by any other Ornstein-Zernike integral scheme we are aware of with comparable computational simplicity. Also, for less strongly repulsive macroions, where the finite core matters, the MPB-RMSA pair structure functions are in good agreement with results from the computationally far more elaborate RY scheme and MC simulations. We show that the degree of thermodynamic inconsistency is reduced in going from the RMSA to the MPB-RMSA solution.

In addition, we compare the MPB-RMSA results for $S(q)$ with static light scattering experiments, which we have performed on suspensions of charged silica spheres in an organic solvent. This serves to demonstrate the applicability of the HSY-DLVO model to experimental systems. That the MPB-RMSA is well suited for extensive parameter scans, is demonstrated in Sec. IV where we study the concentration scaling of the pair structure functions of strongly charged particles at various salt contents. Using the empirical Hansen-Verlet freezing rule, we determine the fluid-solid coexistence line and the fluid-phase regimes in the $(\tilde{T}, \tilde{k}, \phi)$ space, for the class of systems with hard-core interactions masked by the longer-ranged Yukawa repulsion. Here, $\tilde{T}$ is a reduced temperature related to $\tilde{\gamma}$ and $\tilde{k}$. Our conclusions are given in Sec. V.

II. SIZE RESCALING AND IMPROVED RMSA SCHEMES

In this section, we briefly summarize the essentials of the RMSA scheme by Hansen and Hayter.[46,54] We discuss the physically motivated particle-background correction (PB-RMSA) of this scheme introduced by Snook and Hayter.[52,53] We proceed to describe a simple modification of the screening parameter entering into the PB-RMSA scheme which further improves the accuracy.

A. Size-rescaled MSA scheme

For the (effective) pair potential $u(r)$ of the HSY model, the task is to determine the radial distribution function $g(r)$, and the static structure factor $S(q)$, related to each other by[3]

$$g(r) = 1 + \frac{1}{2\pi^2 nr} \int_0^\infty dq \, q \, \sin(qr)[S(q) - 1]. \qquad (7)$$

As noted in the introduction, the one-component Ornstein-Zernike equation,

$$h(x) = c(x) + \frac{6\phi}{\pi} \int d\mathbf{x}' \, c(x') h(|\mathbf{x} - \mathbf{x}'|), \qquad (8)$$

allows in combination with the approximate MSA closure $c(x > 1) = -\beta u(x)$, and the zero-overlap condition $h(x < 1) = -1$, where $x = r/\sigma$, to obtain an essentially analytic solution for $S(q)$, and for the Laplace transform of $r g(r)$.[41,43–45,55]

The MSA solution is reasonably accurate for large concentrations and weak Yukawa repulsion. However, it predicts nonphysical negative values of $g(x)$ for strong Yukawa repulsion and low concentrations. This can be readily noticed from the zero-concentration limit, $g_{MSA}(x > 1) = 1 - \beta u(x)$, of the MSA rdf, giving negative values for radial distances where $u(x) > k_B T$. Negative values of $g_{MSA}(x)$ are found additionally also when the RMSA is applied to highly concentrated systems in the supercooled fluid regime at large values of the coupling parameter γ.[56]

Hansen and Hayter[46] have provided a simple rescaling prescription which remedies the shortcoming of the MSA solution for strongly repelling particles where $\beta u(x = 1^+) \gg 1$ and consequently $g(x = 1^+) \approx 0$, i.e., for systems where the hard core plays no role. In the RMSA, one considers in place of the actual system a system of size-inflated spheres of rescaled hard-core diameter $\sigma' = \sigma/s$, and rescaled volume fraction $\phi' = \phi/s^3$, where the inflation parameter s, with $0 < s \leq 1$, is determined by the Gillan condition $g_{MSA}(x' = 1^+; \phi') = 0$ for $x' = x s = r/\sigma'$. The MSA solution provides an analytical expression for the contact value of the rdf, allowing for a straightforward determination of s, e.g., by a Newton-Raphson type method. We adhere to the standard convention of using the same function names for g, c, and h when expressed in differing length units, with the employed units identified by the function argument variable. While performing the hard-core inflation, the concentration n and the Yukawa tail, $u(r > \sigma')$, are left unchanged. This implies that the potential parameters in Eq. (1) must be rescaled with respect to the length unit σ' according to

$$\gamma' = \gamma s \tag{9}$$

$$k' = k/s. \tag{10}$$

The RMSA solution is given by $g_{RMSA}(r) = g_{MSA}(r; \phi', \sigma')$, which by construction is a non-negative function going continuously to zero at $r = \sigma'$. It approximates to reasonable accuracy the rdf of a family of strongly coupled HSY systems of varying particle sizes σ but equal concentration n and Yukawa tail (i.e., equal $\gamma\sigma$ and equal k/σ). Since all members of the family share the same tail $u(r > \sigma')$, they share in particular the same potential value

$$\Gamma_{is} = \beta u(r = d_{is}), \tag{11}$$

at the ion-sphere diameter distance,

$$d_{is} = \left(\frac{6}{\pi n}\right)^{1/3} = \sigma \phi^{-1/3} = \sigma' \phi'^{-1/3}, \tag{12}$$

used in plasma physics as a characteristic length scale.[3] As $k \to 0$, Γ_{is} reduces to the OCP coupling constant. For strongly repulsive particles where the RMSA solution applies, the ordering $\sigma < \sigma' < d_{is}$ is fulfilled.

The RMSA is an established method providing structure functions in reasonably good agreement with simulation results and many experimental data on charge-stabilized suspensions. Similar to certain other integral equation schemes including the Percus-Yevick (PY) and HNC approximations, it lacks thermodynamic consistency.[3,51] Another artefact of the RMSA of minor importance is a kink in $g(r)$ at $r = \sigma'$

(see Sec. III) caused by the blowing-up of the diameter. Owing to its simplicity, the RMSA solution has been extensively used for charged globular colloids and proteins. It tends to underestimate the principal peaks of the exact $g(r)$ and $S(q)$ as obtained in simulation calculations, with larger differences for large effective charges Z (see, e.g., Refs. 13, 18, and 57). To obtain quantitative agreement with the simulation-generated peak values of $S(q)$, the employed coupling parameter γ has to be enlarged above its physical value, in the case of charged colloids usually by increasing the effective charge number in Eq. (2). The so adjusted RMSA $S(q)$ is overall in quantitative agreement with its simulation counterpart, and the result from the RY scheme which for the repulsive three-dimensional HSY model has been shown to be highly accurate.

B. PB-RMSA scheme

Being forced to treat γ as an adjustable parameter in RMSA calculations is unsatisfactory, in particular when accurate values of the effective charge number are searched for. To improve the RMSA, Snook and Hayter[52] have proposed a reinterpretation of the coupling and screening parameter based on a penetrating microion background (PB) correction argument. The PB-RMSA scheme by Snook and Hayter is in improved agreement with the simulation structure functions. In the following, we briefly describe the PB-RMSA scheme and critically discuss the motivation of the employed PB correction. We will propose a straightforward modification of the PB-RMSA leading to a further performance improvement. In most considered cases, our MPB-RMSA scheme yields very good results, requiring no adjustment of the coupling parameter to unrealistic values. Specific systems where the MPB-RMSA becomes less accurate are discussed in the following Sec. III, with a summary of approximate global error bounds given in the conclusions.

At this point already we stress that the PB correction, underlying the PB-RMSA and the modified PB-RMSA, is neither rigorous nor without alternatives. It is less general and less justified than the hard-core rescaling argument discussed before. Nevertheless, the PB correction improves significantly the performance of the RMSA in the full fluid parameter space.

The PB correction argument by Snook and Hayter relies on the observation that in the derivation of the effective DLVO pair potential in Eqs. (1)–(3), the degrees of freedom of all the point-like microions have been integrated out, so that their presence is felt only through the values for Z and k. Snook and Hayter[52,53] argue, in the spirit of the one-component plasma model (see Ref. 1), that this is consistent with assuming vanishing spatial correlations,

$$g_{Ci}(r) \equiv 1 \quad \text{and} \quad g_{ij}(r) \equiv 1, \tag{13}$$

between colloids and microions, and between all microion species. Here, $g_{Ci}(r)$ and $g_{ij}(r)$ are, respectively, the colloid (C)—microion and microion-microion radial distribution functions, with indices i and j labeling the various microionic species. According to Eq. (13), the microions are uniformly smeared out in space, penetrating also the

colloidal hard cores. While inserting Eq. (13) into the multi-component coupled Ornstein-Zernike equations[3] describing a primitive model system leads indeed to a description that couples the colloidal macroion species to itself only, one should notice that a DLVO-type HSY pair potential can be derived without invoking the crude assumption of a uniformly penetrating microion background. This has been shown, e.g., in Refs. 25, 58–60, where the non-negligible interionic correlations are described more realistically using combinations of MSA and HNC closure relations, respecting the hard core of the colloids. Note further that Eq. (13) in conjunction with the local electro-neutrality condition[3] results in the prediction that $S(q \to 0) = 0$, which for $k > 0$ is violated by the actual HSY structure factor.

To allow for analytic progress, let us accept the uniform penetrating background assumption in Eq. (13) as a useful first approximation. Then, the total charge of uniformly smeared out added salt ions inside the colloidal cores is zero. The monovalent counterions released from the colloid surfaces, however, lead to a reduction of the total charge inside a colloidal sphere from Z to $Z(1 - \phi)$. For small values of ϕ found in low-salinity charge-stabilized systems, the charge-reduction effect predicted on the basis of Eq. (13) often appears to be negligibly small. However, the systems of masked hard-core interactions must be described by the rescaled version of the MSA which invokes a much larger rescaled volume fraction ϕ'. To correct for the charge reduction within the RMSA picture, the colloid charge number should be enlarged from Z to

$$Z^* = \frac{Z}{1 - \phi'}. \tag{14}$$

Incidentally, a relation analogous to Eq. (14) but with un-rescaled volume fraction, relating the bare macroion charge to the effective one-component one, follows from the primitive model when all direct correlations are treated in MSA, and when the high-temperature limit is taken where $k \ll 1$ and $\gamma \ll 1$.[25,59] Only in this limit of dominating thermal kinetic energy, one is allowed to treat the microions as a uniform, non-penetrating background.[58]

The corrected Z^* substituted into Eq. (2) leads to the enlarged background-corrected coupling parameter

$$\gamma^* = \frac{\gamma'}{(1 - \phi')^2}. \tag{15}$$

If γ^* is used in the RMSA with unchanged screening parameter k', a system is modeled with a pair potential larger than the original one for all distances r. Thus the RMSA screening parameter k' must be corrected (enlarged) as well. Snook and Hayter argue that the background correction $\gamma' \to \gamma^*$ should be accompanied by a screening parameter correction $k' \to k^*$, with $k^* > k'$, performed such that the background-corrected HSY potential $u^*(r)$ remains unchanged at the ion-sphere diameter, i.e., they demand that $\beta u^*(d_{is}) = \Gamma_{is}$, with Γ_{is} according to Eq. (11). This yields the correction

$$k^* = k' - 2\phi'^{1/3} \log(1 - \phi'), \tag{16}$$

in units of the rescaled diameter σ'. The PB correction rules in Eqs. (15) and (16) are easily implemented into the standard
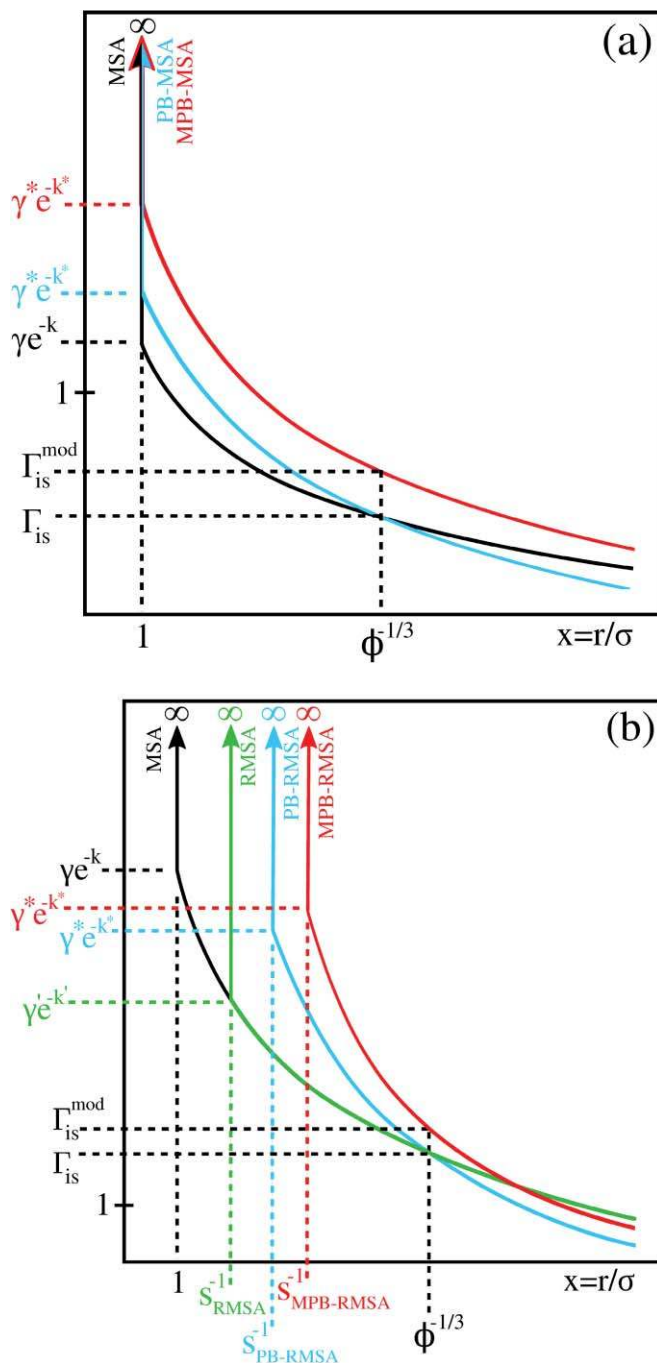

FIG. 1. (a) Sketch of HSY pair potentials in units of $k_B T$ (not to scale) used in the PB-MSA, and MPB-MSA schemes, respectively, for a system requiring no size rescaling. (b) As in (a), but for a system requiring size rescaling. The solid black curve, labeled as MSA, represents the physical pair potential $u(r)$ given by Eqs. (1)–(3). Blue curves: $\beta u^*(x)$; red curves: $\beta u^*_{mod}(x)$. In (b) the indicated $1/s = \sigma'/\sigma$ values are those of the various rescaled diameters σ' in units of the physical diameter σ. Note here that $\sigma < \sigma'_{RMSA} < \sigma'_{PB-RMSA} < \sigma'_{MPB-RMSA} = \sigma^*$.

RMSA algorithm by applying them in each incremental step of the hard-core inflation from the actual value σ to $\sigma' = \sigma/s$, with s determined by the Gillan condition. The rescaled diameter σ' in PB-RMSA is larger than in RMSA, owing to the stronger repulsive forces derived from the steeper potential $u^*(r)$ (see Fig. 1).

By comparison to MC simulations of $g(r)$ for a series of systems with $g(\sigma^+) = 0$, Snook and Hayter have

demonstrated the improved performance of the PB-RMSA relative to that of the RMSA. The PB correction is independent of the hard-core inflation. Therefore it can be applied also in the special case of systems with $g(\sigma^+) > 0$ and $s = 1$. In Sec. III B, we demonstrate that the PB-RMSA for the positive contact value case, which we denote as the PB-MSA, is also of improved accuracy, here in comparison to the unrescaled MSA.

The potential parameters in Eqs. (15) and (16), obtained from the simplifying uniform microion background assumption in Eq. (13), describe a severely altered pair potential as illustrated in Fig. 1. The Yukawa tail of the pair potential $u^*(r)$ used in the PB-RMSA, decays more steeply than the tail of $u(r)$, intersecting the latter at $r = d_{is}$, i.e., at $x = \phi^{-1/3}$. In contrast to the PB-RMSA, the RMSA size-rescaling itself leaves $u(r)$ unchanged not only at the ion-sphere diameter, but for all distances except for the inflated hard-core region which is virtually never probed by the colloids.

There is some ambiguity in selecting d_{is} as the pair distance where the potential value is kept fixed. With equal right, one could select the potential value at the somewhat smaller simple-cubic geometric distance $\tilde{d} = n^{-1/3} \approx 0.8\, d_{is}$. However, results for $g(r)$ and $S(q)$ which we have obtained from our PB-RMSA code using $\tilde{d}$ in place of d_{is}, are of similarly good accuracy in general with no overall improvement. Therefore, following Snook and Hayter, in our PB-RMSA code we shall keep the potential value fixed at $r = d_{is}$.

The PB correction in Eq. (15) is based on the assumption that γ is independent of k. Within the primitive model of charged colloids leading to the effective DLVO potential, on first sight it seems more reasonable to enforce the condition $u^*(d_{is}) = u(d_{is})$ for k^* determined from Eq. (2) in combination with Eq. (14). The resulting variant of the PB-RMSA, which we denote as the implicit PB-RMSA, gives an implicit equation for k^*, the solution of which can be expressed in terms of Lambert's W-function. The k^* and γ^* values of the implicit PB-RMSA are larger than the values given by Eqs. (15) and (16), therefore describing a steeper pair potential. We have tested the performance of the implicit PB-RMSA, finding that as a consequence of the steeper $u^*(r)$, the RMSA-typical underestimation of the peak values in $S(q)$ and $g(r)$ is rendered into a severe overestimation. For this reason, the implicit PR-RMSA has to be dismissed.

In view of the inadequacy of the uniform background assumption and the discussed ambiguities in formulating the PB-correction of $u(r)$, we conclude that the PB-RMSA is justified in essence only by its success in improving the performance of the RMSA solution of the HSY model, with the additional benefit of its analytic simplicity.

C. Modified PB-RMSA scheme

The standard PB-RMSA scheme discussed so far improves the accuracy of the underlying RMSA. Yet, for identical physical values of γ and k in the PB-RMSA, RY scheme and MC simulations, we still observe in the PB-RMSA a noticeable underestimation of the principal peaks in $S(q)$ and $g(r)$.

In order to further improve the accuracy of the PB-RMSA scheme, we propose here an additional concentration rescaling motivated by the specific form of the screening parameter k in Eq. (3). As we have noted before, the factor $1/(1 - \phi)$ in Eq. (3) corrects for the free volume accessible to the pointlike (on the scale of the colloids) microions. On the other hand, within the simplifying uniform microion background picture underlying the PB-RMSA, the free volume has been already corrected for in using Eq. (14). Thus, in order to avoid double correction of the screening parameter in doing a PB-RMSA calculation, we propose to replace the screening parameter k in the set of given physical input parameters (k, γ, ϕ) by the modified value

$$k_{mod} = (1 - \phi)k, \qquad (17)$$

where ϕ is the physical volume fraction. This straightforward modification of the input value k constitutes the modified PB-RMSA (MPB-RMSA), which we refer to as the MPB-MSA scheme in the special case of $s = 1$. Figure 1 illustrates that the modified pair potential, $u^*_{mod}(r)$, used in the MPB-RMSA calculation always lies above the PB-RMSA potential $u^*(r)$, so that $u^*_{mod}(d_{is}) = \Gamma^{mod}_{is} > \Gamma_{is}$. Therefore, the rescaled diameter σ^* in the MPB-RMSA scheme is somewhat larger than the rescaled one in the PB-RMSA scheme (see Fig. 1).

With decreasing ϕ the MPB-RMSA solution approaches the PB-RMSA and RMSA solutions. In the limit $\gamma \to 0$ (e.g., $Z \to 0$) or $k \to \infty$, of a vanishing Yukawa tail, the (M)PB-RMSA and RMSA solutions all reduce to the analytic Percus-Yevick solution of neutral hard spheres. The latter is known to give accurate pair functions of hard-sphere systems provided that $\phi \lesssim 0.35$. At larger ϕ, it underestimates $g(\sigma^+)$ and slightly overestimates the principal peak in the structure factor.

The replacement $k \to k_{mod}$ is not based on a rigorous argument. It is only heuristically motivated, and draws its justification from the very good performance of the MPB-RMSA for an arbitrary repulsive HSY system, not restricted to pair potentials of the special DLVO-type. In Sec. III, it will be shown that the MPB-RMSA scheme is in general in excellent agreement with pair structure function results obtained from simulations, RY calculations and light scattering experiments. A comprehensive description of the algorithm used in our MPB-RMSA code is given in the Appendix.

D. Two alternative integral equations

The (M)PB-RMSA schemes are based on the analytic MSA solution for the HSY model. There exist alternative equation schemes which have been applied to the HSY model, but these are in general purely numerical. The most frequently used numerical schemes for charge-stabilized colloids, are the hypernetted chain (HNC)[61] and Rogers-Young[51] methods which are computationally more expensive. Therefore, the HNC and RY methods should be preferred over the MPB-RMSA only if a significant gain in accuracy is achieved. As we will show in Sec. III, this requirement rules out the HNC method for most of the HSY systems we have studied. The HNC approximation underestimates systematically the principal peak values both in $S(q)$ and $g(r)$, while only mildly

improving the performance over the numerically much faster RMSA. Aside from not showing the nonphysical kink in $g(r)$ at $r = \sigma'$ predicted by the MPB-RMSA (as well as by the PB-RMSA and the RMSA), we did not find system parameters $\{\sigma, \gamma, k, \phi\}$ for which the accuracy of the HNC comes up to that of the MPB-RMSA.

The elaborate RY method has been found, from comparison with simulation results of $S(q)$ and $g(r)$, to perform excellently for the repulsive HSY model. We have confirmed this finding for all considered systems covering a broad range of system parameters.

We have used the standard RY scheme which interpolates continuously between the PY closure at short and the HNC closure at long distances, by a single-parameter mixing function. The RY hybrid closure is motivated by the observation made for the repulsive HSY potential, and for purely repulsive inverse power potentials, that the exact $S(q)$ is bracketed at small q and at the principal peak position by the PY and HNC predictions. The RY mixing parameter is determined by imposing local thermodynamic self-consistency, i.e., by enforcing equality between the compressibility equation of state

$$\lim_{q \to 0} S(q) = k_B T \left(\frac{\partial n}{\partial p} \right)_T, \tag{18}$$

and the compressibility obtained from the density (concentration) derivative of the virial pressure

$$p_v = n k_B T - \frac{2\pi}{3} n^2 \int_0^\infty dr \, r^3 \, g(r) \frac{\partial u(r)}{\partial r}. \tag{19}$$

In taking the density derivative, the weak density dependence of the mixing parameter is disregarded (imposing local consistency only), and for colloids also the concentration dependence of the effective pair potential. For colloids, $S(0) := \lim_{q \to 0} S(q)$ relates to the osmotic isothermal compressibility. How precisely a state-dependent effective pair potential modifies the pressure, energy and compressibility equations of state is a subtle question still under debate.[62–69] The present work is concerned with the pair structure in HSY fluids only, not addressing its relation to the thermodynamic properties of systems with state-dependent interactions.

Different from the RY scheme, the (M)PB-RMSA and HNC methods are thermodynamically inconsistent. Owing to its local thermodynamic consistency, the RY scheme is expected to give accurate values of $S(q)$ in particular at small q. We use the RY scheme to test the predictions of the MPB-RMSA for $S(0)$, and to quantify the improvement in thermodynamic consistency in going from the RMSA to the MPB-RMSA scheme.

A general conclusion drawn from the comparison of the MPB-RMSA and RY scheme structure functions with MC data described in the following section, is that the static structure factor is nearly always predicted with excellent accuracy by both methods for same input parameters, while a remnant principal peak underestimation in $g(r)$ is found in case of the MPB-RMSA. Recall, however, that the computational load of the RY scheme is much higher. Moreover, it does not give analytic expressions for $S(q)$ and $g(r)$ which could be used, e.g., as input into dynamic theories.

III. PERFORMANCE OF THE MPB-RMSA

The integral equation and MC simulation results discussed in this section have been obtained using a HSY pair potential in the form of Eqs. (1)–(3) which describe the electrosteric repulsion of microion-dressed colloidal macroions. We have tested the performance of various integral equation schemes, most notably here the (M)PB-RMSA, in comparison to MC results, and static light scattering (SLS) data from suspensions of charged silica spheres. Systems with a broad range of interaction parameters have been examined, from systems with strong Yukawa repulsion close to freezing down to systems with a weak Yukawa tail where the physical hard core plays a role. Only a representative selection of results is shown here, for different values of ϕ, n_s, L_B/σ and Z which are to some extent under experimental control. The MC simulations were performed using in general $N = 512$ particles placed in a periodically repeated cubic simulation box. In strongly correlated particle systems with long-range Yukawa repulsion, a larger number $N = 800$ was used, for improved statistics and resolution of the principal peak region of $S(q)$. We first discuss systems with strong Yukawa repulsion. Next, systems with a weak Yukawa tail are considered. Moreover, we test the degree of thermodynamic consistency of the considered integral equation schemes.

A. Systems with strong Yukawa repulsion

Systems with strong Yukawa repulsion, where $\beta u(\sigma^+) = \gamma \exp\{-k\} \gg 1$, are characterized by a (practically) zero likelihood for contact configurations so that the hard core plays no role. Strong Yukawa repulsion of colloidal particles is observed for large charge numbers and sufficiently low salt concentrations.

1. Integral equations in comparison to MC simulations

As a representative class of colloidal systems with strong and long-range Yukawa repulsion, we consider spheres of diameter $\sigma = 200$ nm and effective charge number $Z = 100$, immersed under zero-added salt conditions ($n_s = 0$) in a weakly polarizable solvent ($\epsilon = 10$, $T = 297$ K) of Bjerrum length $L_B = 5.62$ nm. For these parameters, the reduced potential at contact is typically quite large, e.g., $\beta u(\sigma^+) = 260$ for $\phi = 10^{-4}$. Figure 2 shows our integral equations and MC simulation results for $S(q)$ and $g(r)$ at various volume fractions, and Z assumed to be concentration independent. We will exemplify further down that Z is in general ϕ-dependent for an actual experimental system. The considered volume fractions cover the range from dilute systems with moderate particle correlations to more concentrated systems with strong pair correlations.

The depicted RMSA curves are in fair qualitative agreement with the MC-generated pair structure functions. As expected, the RMSA underestimates the principal peak heights, $S(q_m)$ and $g(r_m)$, at the positions q_m and r_m, respectively. The HNC approximation improves only slightly the accuracy of the RMSA. The RY-scheme, on the other hand, is in excellent agreement with the MC data at all considered ϕ. It slightly
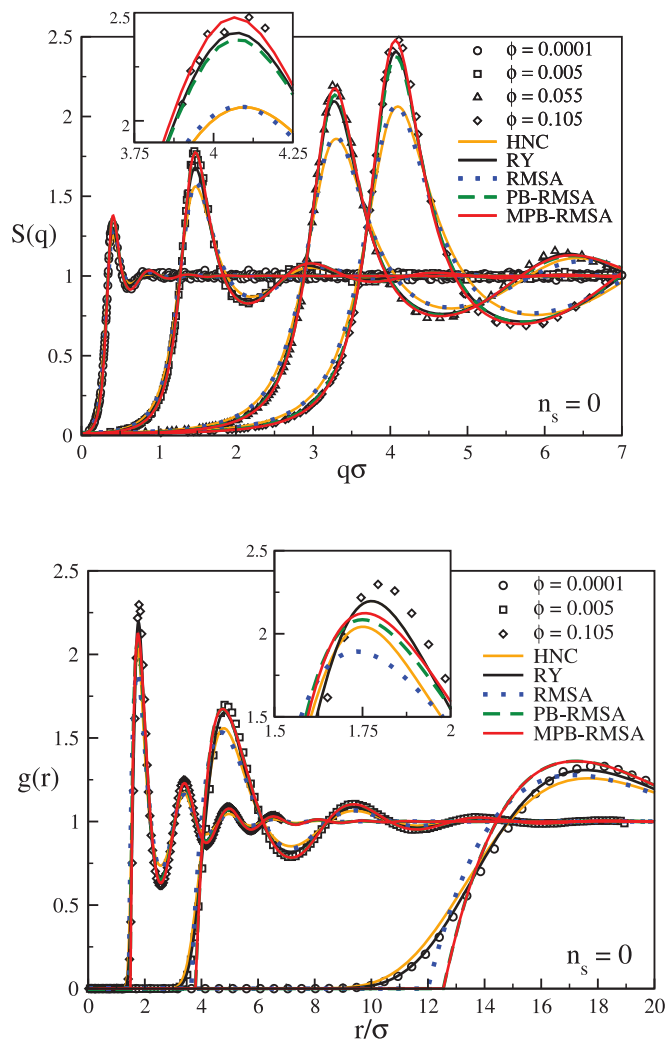
FIG. 2. Static structure factor, $S(q)$, and radial distribution function, $g(r)$, of a zero-salinity system at volume fractions ϕ as indicated. Open symbols are MC simulation data in comparison with various integral equation scheme predictions as indicated. The insets magnify the principal peak regions of the most concentrated system. System parameters are: $Z = 100$, $L_B = 5.62$ nm, $\sigma = 200$ nm, zero added salt.
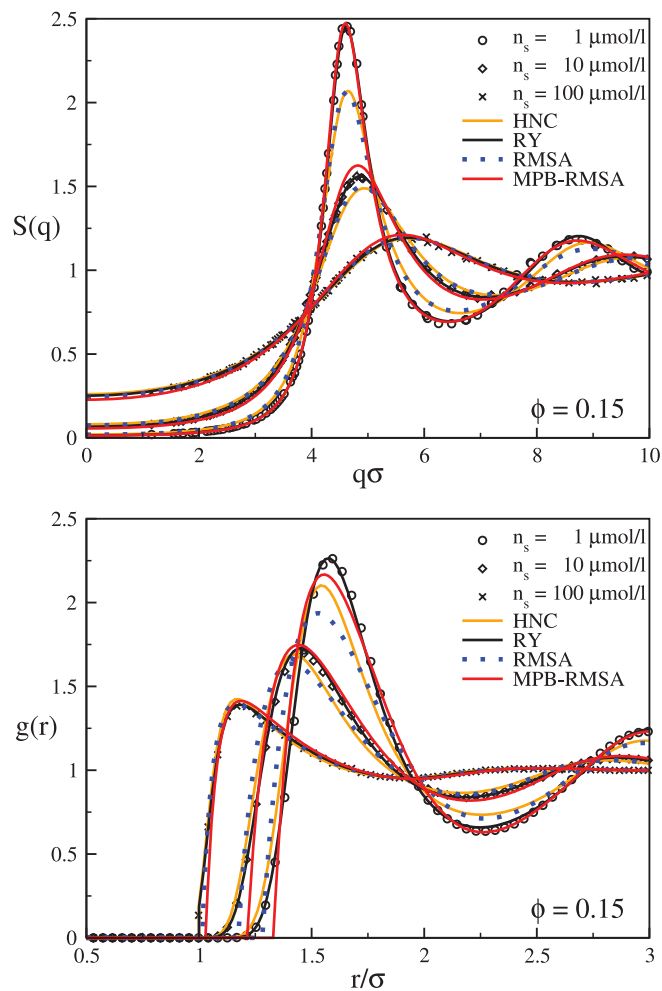

FIG. 3. Static structure factor, $S(q)$, and radial distribution function, $g(r)$, at various salt concentrations, n_s, as indicated. Symbols represent MC simulation data. System parameters as in Fig. 2, except now for a higher volume fraction $\phi = 0.15$ and nonzero concentrations of added 1-1 electrolyte.

underestimates the MC-$S(q_m)$ for the largest concentration only.

The MPB-RMSA and PB-RMSA schemes are in very good overall agreement with the MC results, except for a kink in $g(r)$ at the rescaled diameter which is most noticeable at low concentrations, and except for a slight underestimation of the principal peak value $g(r_m)$ at larger ϕ. The MPB-RMSA and the PB-RMSA coincide for low ϕ but, as a general rule, the MPB-RMSA performs better at larger volume fractions. For this reason, in the following figures we only include the results from the modified MPB-RMSA. At $\phi = 0.105$, the MPB-RMSA happens to predict a principal peak height, $S(q_m)$, in even better agreement with the simulation data than the RY scheme.

The discussed characteristics of the considered integral equation schemes persist when the concentration, n_s, of added 1-1 electrolyte is increased. This is demonstrated in Figs. 3 and 4 for a concentrated ($\phi = 0.15$) and dilute ($\phi = 0.055$) system, respectively. Consider first the system in

Fig. 3 which is more concentrated than the most concentrated one in Fig. 2, but approximately with the same peak height $S(q_m) \approx 2.5$. This is due to the small amount, $n_s = 1$ μmol/l, of added salt which for the present system is large enough to cause significant additional screening. According to Eq. (3), the square of the screening parameter is the sum

$$k^2 = k_c^2 + k_s^2, \tag{20}$$

of a contribution, k_c^2, proportional to Z and arising from the surface-released monovalent counterions, and a second contribution, k_s^2, due to added salt ions. The cross-over from surface-counterion to salt-ion dominated screening occurs at $\phi \sim \pi n_s \sigma^3/(3|Z|)$, or equivalently at

$$n_c \sim 2n_s, \tag{21}$$

where $n_c = n|Z|$ is the concentration of surface-released, monovalent counterions. The cross-over volume fraction at $n_s = 1$ μmol/l is quite close to the considered system volume fraction of $\phi = 0.15$. The added-salt systems in Figs. 3 and 4 exemplify our general observation that the MPB-RMSA slightly overestimates the pair ordering at
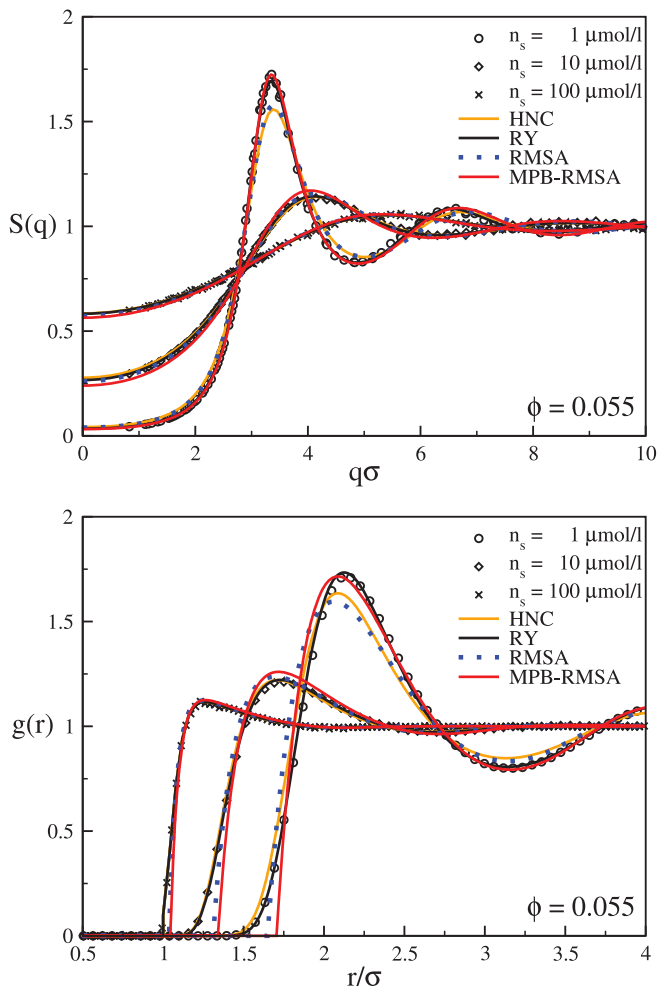
FIG. 4.   Same as in Fig. 3 but for a small volume fraction of $\phi = 0.055$.

FIG. 5. Static structure factor, of $S(q)$, of TPM-coated, charged silica spheres dispersed in a toluene-ethanol mixture. Triangles are the static light scattering data. Physical parameters used in the calculations are: L_B = 8.64 nm, $\sigma = 272$ nm and $n_s = 0.7$ μmol/l. The charge numbers determined from fitting the experimental data, are identical for the MC, RY, and MPB-RMSA methods, namely $Z = (135, 190)$ for $\phi = (0.057, 0.15)$. The nonmodified PB-RMSA predicts different values, namely $Z = (145, 300)$.

intermediate salt concentrations, and this more so at lower volume fractions. We have confirmed this by calculations at various intermediate volume fractions for which the results are not shown here. At the largest salinity $n_s = 100$ μmol/l considered in Figs. 3 and 4, both the RY and HNC scheme predict a small but non-zero contact value, whereas $g(\sigma^+) = 0$ according to the MSA-based schemes. Except for the narrow interval at $r \approx \sigma$, the $g(r)$'s of all integral equation schemes agree with each other in the high-salinity case. The rdf in Fig. 4 for $n_s = 100$ μmol/l has a visible maximum $g(r_m) > 1$ at the next-neighbor shell distance $r_m \approx 1.2 \times \sigma$. This clearly distinguishes it from the infinite dilution limit, $g_0(r) = \exp\{-\beta u(r)\}$, which exhibits no maximum at finite r.

2. Comparison with experiment

The high accuracy of the MPB-RMSA for systems of strongly correlated particles points to its capability as a conveniently fast tool for evaluating scattering data. To illustrate this, we use the MPB-RMSA in the following to fit experimental $S(q)$ which we have obtained from static light scattering (SLS) experiments on suspensions of negatively charged trimethoxysilylpropyl methacrylate (TPM)-
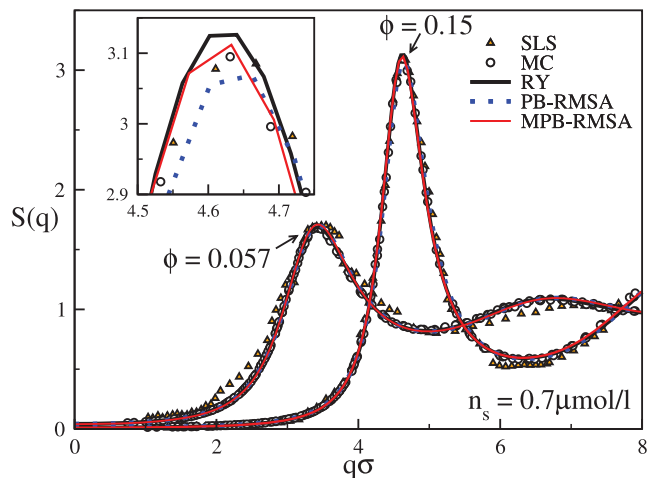
coated silica spheres,[70] dispersed in an index-matching 80:20 toluene-ethanol solvent mixture at $T = 20^o$ C and $L_B = 8.64$ nm.[15] The organic solvent mixture allows for fine-tuning of the salinity without having to worry about self-dissociation of solvent molecules and uncontrolled CO_2 adsorption, problems encountered for in aqueous suspensions. Moreover, the index matching minimizes the influence of residual van der Waals attraction. The particle diameter determined by small-angle x-ray scattering is $\sigma = 272$ nm, and the relative size polydispersity is 0.06. For a residual salinity smaller than 1μmol/l, the suspension freezes at $\phi \approx 0.16$ where the experimental $S(q)$ attains a principal peak value of about 3.2. The SLS experiments were conducted using a light scattering set-up by the ALV-Laservertriebsgesellschaft (Langen, Germany), for a series of concentrations from $\phi = 0.057$ to $\phi = 0.159$. We carefully filtered the system and checked that there is no noticeable multiple scattering. The scattering data are consequently quite reliable, and of little noise even in the small wavenumber regime. The residual salinity $n_s = 0.7 \mu$mol/l in the system was determined as a global fit-parameter from a concentration series of SLS measurements of $S(q)$, fitted by the MC, RY, and MPB-RMSA calculations. The only ϕ-dependent fitting parameter in our analysis has been the effective charge number Z, which was adjusted in each of the employed methods to match the experimental $S(q_m)$.

Figure 5 exemplifies our theoretical analysis of the concentration series experiments by showing the peak-height adjusted $S(q)$ of the MC, RY, and (M)PB-RMSA methods, for the least concentrated system ($\phi = 0.057$) in the series, and a concentrated system ($\phi = 0.15$) close to the freezing transition. The fraction of surface-released counterions is large enough even at $\phi = 0.057$, with $k_c = 0.93 \times k_s$, to guarantee a small value for the osmotic compressibility. All three methods considered in Fig. 5 reproduce the experimental $S(q)$ with excellent accuracy in the whole experimentally accessible
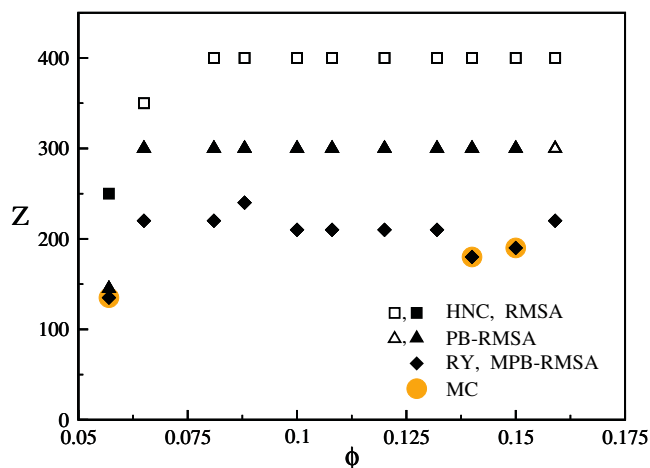
FIG. 6. Effective charge number Z used in various schemes for a best approximation of the SLS $S(q_m)$ in the concentration series of charged silica spheres in a toluene-ethanol mixture. Common parameters are : $L_B = 8.64$ nm, $\sigma = 272$ nm, and $n_s = 0.7$ μmol/l. Shaded circles: MC simulations. Diamonds: RY and MPB-RMSA results. Triangles: PB-RMSA. Squares: HNC and RMSA. Filled symbols are used when the experimental $S(q_m)$ could be reproduced, and open symbols when it is underestimated for any Z. In the latter case, the lowest Z is plotted which minimizes the peak-height underestimation.

q-range. In Fig. 6, the deduced effective charges are plotted for the complete concentration series. Interestingly enough, the MC, RY, and MPB-RMSA methods all give the same values for the effective charges, with uncertainties comparable to the symbol sizes. This highlights the capability of the MPB-RMSA to deliver reliable results for the effective charge with little numerical effort. In contrast, the (unmodified) PB-RMSA version of Snook and Hayter overpredicts the values of Z systematically, but not to such an extent as the HNC and RMSA schemes which overestimate the effective charge of the silica spheres roughly by a factor of two, giving practically coincidental values (see Fig. 6).

The RMSA and HNC peak values of $S(q)$ for $\phi > 0.06$ could not be made large enough to reach the experimental peak heights, for any reasonable value of Z. For the most concentrated system ($\phi = 0.159$) right at the freezing point, even the PB-RMSA calculated $S(q_m)$ remains well below the experimental $S(q_m)$, for any value of Z. This inability of the RMSA and HNC schemes to reach the experimental peak heights in certain low-salinity systems, like the considered silica samples, can be explained by the competing influence of added salt ions and surface-released counterions [see Eq. (20)]: when Z is increased from small values at a given ϕ, $S(q_m)$ increases initially since γ increases with Z for nearly constant k, as long as $n_c \ll n_s$. When Z becomes large, however, the cross-over point described by Eq. (21) is surpassed, and the surface-released counterions start to dominate the electrostatic screening. Then, $S(q_m)$ decreases with increasing Z since the effect of the increasing coupling parameter γ on the pair structure is overcompensated by the also increasing screening parameter k. Consequently, $S(q_m)$ goes through a maximum as a function of Z. When $S(q_m)$ is calculated by a method such as the RMSA which underestimates the structure of strongly correlated particles, the pre-

dicted maximum of $S(q_m)$ as function of Z may be not large enough to reach the experimental peak value.

In summarizing our discussion of systems with strong Yukawa repulsion, we conclude that out of all considered methods only the RY and MPB-RMSA schemes, and of course the MC simulation method, allow for a fully consistent fit of experimental structure factors, providing trustworthy values for the effective charge.

Out of these three schemes, only the RY and MC methods have been well-established so far, routinely used to fit scattering data. However, the fitting procedure can be quite cumbersome due to the non-analytic nature of these two methods, causing thus long execution times. On a standard desktop PC, one MC run of good statistics typically takes several hours, and about 10 seconds are usually needed for the RY calculated pair structure functions of a given system. An additional complication in applying the RY scheme is caused by its internal iterative algorithm which interpolates between HNC and the Percus-Yevick closure to achieve local thermodynamic consistency. Convergence of this algorithm depends on an initial seed for the mixing parameter which has to be provided by the user. In our experience, it is occasionally difficult to find an appropriate seed that allows the RY-scheme to converge.

The MPB-RMSA code, on the other hand, is rapidly evaluated for any system, with a typical cpu-time of less than 0.1 seconds. This has allowed us to implement the MPB-RMSA with a convenient graphical user interface in which an imported $S(q)$ or $g(r)$ can be readily fitted. Input parameters such as Z and ϕ can be tuned with real-time response of the MPB-RMSA structure functions, resulting in a fast and versatile fitting tool of quantitative accuracy.

B. Systems with nonzero contact values

Complementary to the strong Yukawa coupling regime in the HSY model where $g(\sigma^+) \approx 0$, there is the regime of weak Yukawa repulsion characterized by non-zero contact values. For weak Yukawa coupling is $\gamma e^{-k} \lesssim 1$, which for the DLVO parameters in Eqs. (2) and (3) holds true for a sufficiently low Z and sufficiently large salt content. Even for a nonzero probability of two macroions in contact, where $g(\sigma^+) > 0$, in many cases there is still a principal maximum $g(r_m) > g(\sigma^+)$ at $r_m/\sigma > 1$ caused by the Yukawa tail. This clearly distinguishes these systems from neutral hard-sphere suspensions where $\gamma = 0$ or $k = \infty$ (see Fig. 8 for an example). HSY systems with nonzero contact values are difficult to realize experimentally, since for colloids, e.g., one needs to worry about residual van der Waals forces which become strong at contact. Irrespective of any experimental realization, it is of interest to test the performance of the (M)PB-MSA under conditions where no rescaling is required. We do this in the following by comparison with MC simulations and RY calculations.

We start by investigating the contact value of the rdf which, in the weak coupling regime, is an indicator for the accuracy of an integral equation scheme. In Fig. 7, we present results for $g(\sigma^+)$ by the various integral equation schemes in comparison with MC data. The system parameters are representative of a low-salinity, aqueous solution of nano-sized
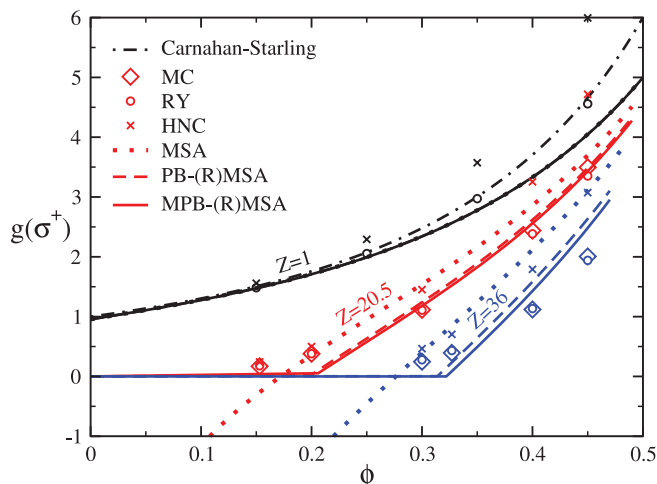
FIG. 7. Contact value of $g(r)$ obtained by MC simulation (diamonds), RY (circles), HNC (crosses), MSA (dotted lines), PB-(R)MSA (dashed lines), and MPB-(R)MSA (solid lines). Black (top): $Z = 1$, red (middle): $Z = 20.5$, blue (bottom): $Z = 36$. Dashed-dotted black line: Carnahan-Starling contact value for hard spheres. Common parameters: $L_B = 0.71$ nm, $\sigma = 13.8$ nm, $n_s = 10$ μmol/l.

apoferritin proteins.[18] Three different effective charge numbers, $Z = 36$, 20.5 and 1, are considered.

For $Z = 1$, the limit of neutral hard spheres (HS) is reached practically, with tiny differences to the hard-sphere contact value only. For hard spheres, $g_{HS}(\sigma^+) = (1 - 0.5\phi)/(1 - \phi)^3$ as derived from the Carnahan-Starling equation of state.[3] In the limit of zero Yukawa coupling ($Z = 0$), the (M)PB-MSA and the MSA reduce to the Percus-Yevick solution for hard spheres, which is known to underestimate the exact $g_{HS}(\sigma^+)$ at larger volume fractions ($\phi \gtrsim 0.35$). On the other hand, the RY predictions for $g(r)$ including the contact values are in excellent accord with the MC simulation results, for all considered values of Z (see Fig. 8). The HNC is known to deteriorate in its performance when systems with shorter-range repulsive potentials are considered, predicting a too pronounced next neighbor shell and a too large contact value of the rdf.
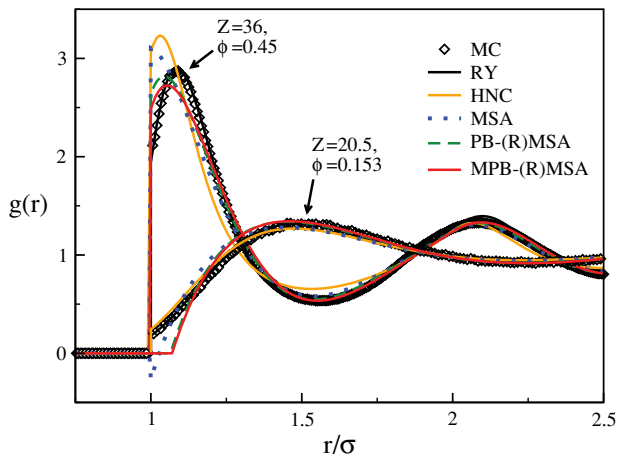

FIG. 8. Radial distribution function for two systems selected from Fig. 7. Common parameters: $L_B = 0.71$ nm, $\sigma = 13.8$ nm, $n_s = 10$ μmol/l. Charge numbers and volume fractions as indicated.

The supremacy of the (M)PB-MSA schemes over the MSA in the no-rescaling regime of positive contact values shows up more clearly when the charge number is increased so that the electrostatic and excluded volume interactions are of comparable importance. An analysis of a large number of systems with finite contact values at various charge numbers, hard-core diameters, and electrolyte concentrations has revealed that all three MSA-based schemes tend to overestimate the increase of $g(\sigma^+)$ with increasing ϕ as obtained by the MC and RY methods, whenever $\gamma e^{-k} \gtrsim 3.0$. Among the MSA-based schemes, the weakest overestimation is observed for the MPB-RMSA method. See here for example the system with $Z = 36$ in Fig. 7. Consider next the $g(r)$ of a dense system at $\phi = 0.45$ and $Z = 36$ depicted in Fig. 8. For this system, $g(\sigma^+) = 2.01$, 2.48 and 2.64 in MC, MPB-MSA, and PB-MSA, respectively. While the MPB-MSA performs better than the PB-MSA regarding the contact value, the primary Yukawa-tail peak of $g(r)$ at $r_m > \sigma$ is slightly more underestimated by the modified PB-MSA version. A general observation for systems with weak Yukawa coupling is that, while contact values and Yukawa-tail induced peak values are not precisely reproduced, the overall shape of the (M)PB-MSA $g(r)$ is still in good accord with the MC and RY results.

C. Test of thermodynamic consistency

Out of all integral schemes considered in this work, the RY scheme is the only one which is thermodynamically self-consistent regarding the (osmotic) compressibility. By construction, the zero-q limiting value of the inverse RY static structure factor agrees with the concentration derivative, $\beta (\partial p_v/\partial n)_T$, of the virial pressure in Eq. (19). In taking the derivative, a possible concentration dependence of $u(r)$ and of the mixing parameter has been ignored (see discussion in Sec. II D).

We can use the RY results for $S(0)$ as accurate reference values to quantify the degree of thermodynamic inconsistency for each of the other considered integral equation schemes, by comparing the results for $S(0)$ with those for $k_B T (\partial n/\partial p_v)_T$, the latter obtained by a numerical differentiation of the virial pressure p_v as in the RY case.

In a HSY system with strong and long-range Yukawa repulsion, $S(0)$ attains values close to zero. Therefore, to clearly see differences, in Fig. 9 we plot the predictions for $1/S(0)$ (solid lines) by the various integral equation schemes along with the corresponding results for $\beta (\partial p_v/\partial n)_T$ (dashed lines). The system parameters of $L_B = 8.64$ nm, $\sigma = 200$ nm, $n_s = 1$ μmol/l, and $Z = 200$ are representative of a low-salinity system of strongly repelling macroions. The volume fraction interval covers the complete fluid-phase regime up to $\phi = 0.15$, with a peak height $S(q_m) \approx 3.1$ where, according to the empirical Hansen-Verlet freezing rule, systems with long-range Yukawa repulsion are close to the freezing point.[36,71,72]

In Fig. 9, it can be noted that all considered integral equation schemes except the RY are thermodynamically inconsistent, with the relative difference between compressibility and virial results extending up to 53% for the HNC, 45% for the RMSA, 34% for the PB-RMSA and 24% for the MPB-RMSA. The self-consistent RY result for the inverse
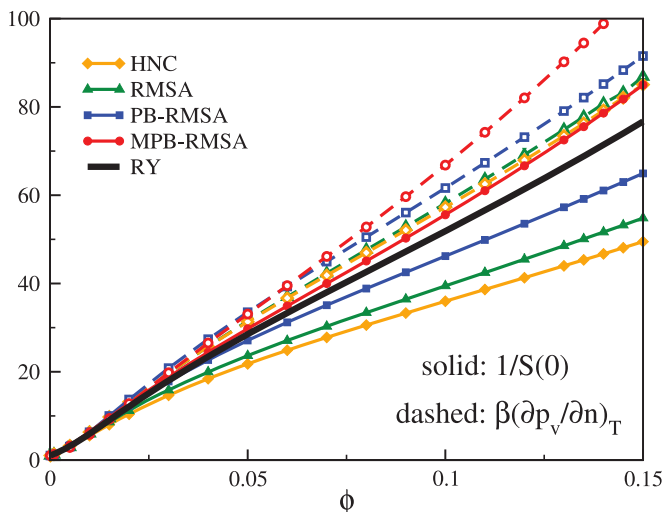
FIG. 9. Test of local thermodynamic consistency. Solid lines with filled symbols: $1/S(0)$ as a function of ϕ, for different integral equation schemes as indicated. Dashed lines with open symbols: corresponding predictions for $\beta(\partial p_v/\partial n)_T$, obtained from the concentration derivative of the virial pressure in Eq. (19). System parameters: $L_B = 8.64$ nm, $\sigma = 200$ nm, $n_s = 1$ μmol/l, $Z = 200$.

reduced compressibility is bracketed by the HNC, RMSA and PB-RMSA solutions, but not by the MPB-RMSA results. The predictions for $1/S(0)$ by the various schemes grow roughly linear in concentration for all $\phi > 0.025$, where the lower bound is the concentration value for which $k_s = k_c$.

Figure 9 shows that, as a consequence of the improvement of the RMSA-predicted pair structure by the modified PB correction, also the degree of thermodynamic consistency is improved. Unlike HNC and RMSA, the MPB-RMSA result for $S(0)$ is in reasonably good accord with the RY result even up to the freezing concentration. Thus, the MPB-RMSA can be used to obtain a quick estimate of the (osmotic) compressibility. However, if quantitative accuracy is required, the RY-method is the method of choice.

IV. CONCENTRATION SCALING AND FLUID-PHASE BEHAVIOR

Having established the good accuracy of the MPB-RMSA in comparison to MC and RY calculations, we demonstrate now its capability as a fast tool to explore generic features in the pair structure and fluid-phase behavior of HSY systems. The explorations discussed below have required extensive parameter scans. We focus in the following again on systems with strong Yukawa repulsion characterized by $g(\sigma^+) \approx 0$.

As a first application of the MPB-RMSA, in Fig. 10 we investigate the generic concentration dependence of the principal peak positions r_m and q_m of $g(r)$ and $S(q)$, respectively, for suspensions of strongly charged colloidal macroions. For these systems, one expects that the particles minimize their configurational free energy by maximizing the radius of the next-neighbor shells. Thus, r_m should scale geometrically in concentration according to $r_m \sim \tilde{d} = n^{-1/3}$, and q_m according to $q_m \sim 2\pi/\tilde{d}$.
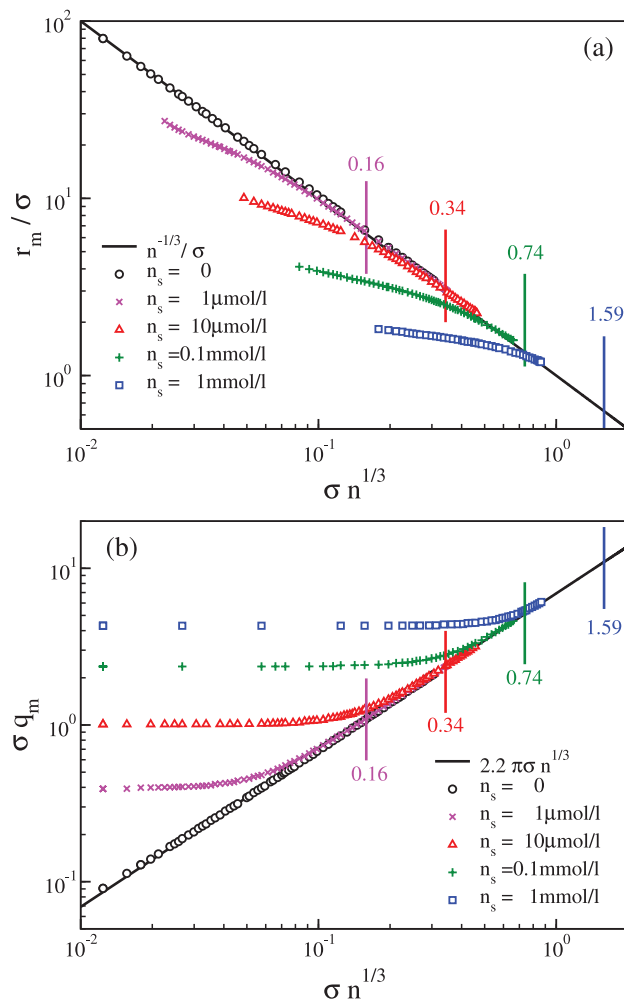

FIG. 10. (a) Radial position, r_m, of the principal maximum in $g(r)$, and (b) wavenumber location, q_m, of the principal maximum in $S(q)$, plotted versus the inverse geometric pair distance $1/\tilde{d} = n^{1/3}$ in units of σ. Results for various salt contents (as indicated) were generated using the MPB-RMSA. Abscissa values where $k_s = k_c$ are marked by vertical lines. Parameters $L_B = 0.716$ nm, $\sigma = 100$ nm, and $Z = 300$ are representative of an aqueous suspension of strongly charged macroions.

Figure 10 demonstrates that the scaling relations $r_m = \tilde{d}$, and $q_m = 1.1 \times 2\pi/\tilde{d}$, are obeyed to good accuracy, provided the salt concentration n_s is not too large and the volume fraction is not too low. In the experimentally not realizable case of zero salinity ($n_s = 0$), the geometric scaling of the peak positions with the colloid concentration remains valid down to very low values of n. With increasing salt content, the concentration of salt ions eventually surpasses the concentration of surface-released counterions, leading to a significant reduction in the reduced Debye screening length, $1/k$, and the pair potential contact value at $r = \sigma$. This softens the Yukawa tail, allowing two particles to come closer than $n^{-1/3}$, indicated in Fig. (10) by deviations of r_m and q_m from the $n^{\pm 1/3}$ scaling behavior. As a crude criterion for the transition to geometric concentration scaling behavior, we can use $k_c > k_s$, or equivalently, $n > 2n_s/|Z|$, where k_c according to Eq. (20) is the contribution to k due to the monovalent counterions released from the colloid surfaces. This simple criterion is qualitatively confirmed in Fig. 10 where the colloid
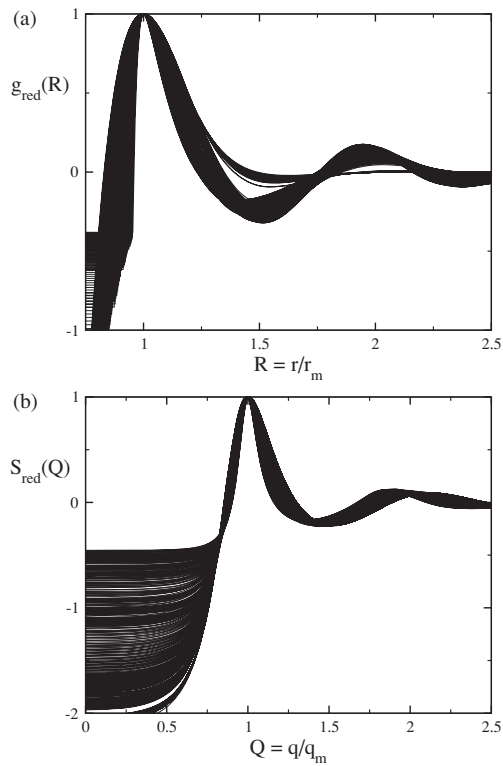
FIG. 11. (a) Reduced radial distribution function $g_{\text{red}}(R)$, and (b) reduced static structure factor $S_{\text{red}}(Q)$, for a large number of systems with $\phi = 0.01$, $g_{\text{MPB-RMSA}}(\sigma^+) = 0$ and $S(q_m) \leq 3.2$. Systems in (a) satisfy additionally that $0.99 \leq r_m/\tilde{d} \leq 1.01$, and in (b) that $0.99 \leq q_m\tilde{d}/(2.2\pi) \leq 1.01$.

concentrations where $n = 2n_s/|Z|$ are marked by short vertical lines. Note that the geometric scaling of r_m necessarily fails at very high concentrations where $\tilde{d}$ approaches σ.

For systems where r_m and q_m obey geometric concentration scaling, one might anticipate that the reduced pair structure functions

$$g_{\text{red}}(R) = \frac{g(r/r_m) - 1}{g(r_m) - 1}, \tag{22}$$

$$S_{\text{red}}(Q) = \frac{S(q/q_m) - 1}{S(q_m) - 1}, \tag{23}$$

with $R = r/r_m$ and $Q = q/q_m$, are approximately universal except for small values of their arguments. By definition, $g_{\text{red}}(R)$ and $S_{\text{red}}(Q)$ are equal to one at $R = Q = 1$ and converge to zero for both $R, Q \to \infty$. The function $S_{\text{red}}(Q)$ is nonuniversal at $Q \approx 0$, since even for the subclass of low-compressibility systems where $S(0) \approx 0$ and $S_{\text{red}}(0) \approx -1/(S(q_m) - 1)$, different values for $S_{\text{red}}(0)$ are obtained for different principal peak heights. By the same token, $g_{\text{red}}(R)$ behaves nonuniversal at $R \approx 0$.

In Fig. 11, MPB-RMSA results for $g_{\text{red}}(R)$ and $S_{\text{red}}(Q)$ are displayed for a large number of fluid-ordered HSY systems with $S(q_m) \leq 3.2$, masked hard-core interactions, and geometric concentration scaling of r_m and q_m, respectively. There are pronounced variations in the width of the principal peaks and in the undulations of the following minimum and maximum. The sharpest peaks are found for the most strongly structured, low-compressibility systems. These systems show additionally the largest values of $g_{\text{red}}(0)$ and $S_{\text{red}}(0)$. The

figure clearly illustrates that the reduced structure functions are non-universal even away from the small argument regime.

According to Eq. (7), a universal $g_{\text{red}}(R)$ for systems where $r_m = \tilde{d}$ would imply a linear relationship between $S(q_m) - 1$ and $g(r_m) - 1$. This would allow the rephrasing of the Hansen-Verlet freezing criterion for $S(q_m)$ in terms of $g(r_m)$. However, such a simple 1-1 relation between $S(q_m)$ and $g(r_m)$ does not exist in general. This will be explicitly demonstrated as a by-product of the following discussion.

Up to this point, parameters including ϕ, $n_s\sigma^3$ and L_B/σ have been varied which are to a certain extent under experimental control. However, as noted in the introduction, strong Yukawa systems for which $g(\sigma^+) \approx 0$ are fully characterized by two independent coupling parameters, namely $\tilde{\gamma}$ and $\tilde{k}$ appearing in Eq. (4).

In discussions of the phase behavior, it is more convenient to use the pair $(\tilde{T}, \tilde{k})$ in place of $(\tilde{\gamma}, \tilde{k})$, with the reduced temperature

$$\tilde{T} = \frac{k_B T}{u(\tilde{d})} = \frac{\exp(\tilde{k})}{\tilde{\gamma}}, \tag{24}$$

measuring the thermal energy relative to the potential energy of a pair of particles at distance $\tilde{d} = n^{-1/3}$. A given state point $(\tilde{T}, \tilde{k})$ corresponds to a unique $g(r)$ and $S(q)$, for r and q expressed in units of $\tilde{d}$. Different sets, $\{\sigma, L_B/\sigma, Z, n_s\sigma^3, \phi\}$, of experimentally controllable parameters can describe the same state point $(\tilde{T}, \tilde{k})$.

HSY systems with non-negligible finite contact values $g(\sigma^+) > 0$ require three independent parameters to span the phase space. A convenient choice is $(\tilde{T}, \tilde{k}, \phi)$. Systems of equal $(\tilde{T}, \tilde{k}, \phi)$ have the same $S(q)$ and $g(r)$ in common, with q and r expressed in units of σ.

We proceed by discussing the fluid-phase diagram part of HSY systems with masked hard-core interactions, characterized by the two parameters $\tilde{T}$ and $\tilde{k}$. The diagram is constructed using the MPB-RMSA predictions for $S(q_m)$ in combination with the empirical Hansen-Verlet rule. For a neutral hard-sphere system with no long-ranged, soft Yukawa repulsion, the Hansen-Verlet rule states that $S(q_m) = 2.85$ at freezing. Computer simulations[36,71,72] and density functional theory calculations[73] have shown that $S(q_m)$ at freezing varies between 2.85 and 3.3 for HSY systems, depending on the range of the Yukawa tail. In the present study, a fixed value of 3.2 was selected for simplicity, in agreement with the freezing peak value of $S(q)$ found experimentally in our low-salinity charged silica system.

Figure 12 shows our result for the $\tilde{T} - \tilde{k}$ phase diagram for a very extended range, $\tilde{T} = 10^{-3} - 10^{10}$ and $\tilde{k} = 10^{-4} - 50$, of state points. Fluid-phase systems are characterized by peak values $S(q_m) < 3.2$. The inset shows the lower-$\tilde{k}$ part of the diagram on a linear scale. A uniformly colored areal segment in the diagram includes the state points of fluid systems of equal volume fraction. Seven different volume fractions ϕ from 0.01 to 0.45 are considered. An areal segment of given ϕ is bounded from above by the line determined from $g_{\text{MPB-RMSA}}(\sigma^+; \phi) = 0$, and from below by the freezing line $S(q_m) = 3.2$ common to all segments. Thus, for instance the green area describing the $\phi = 0.01$ systems extends all the way down to the freezing line separating the
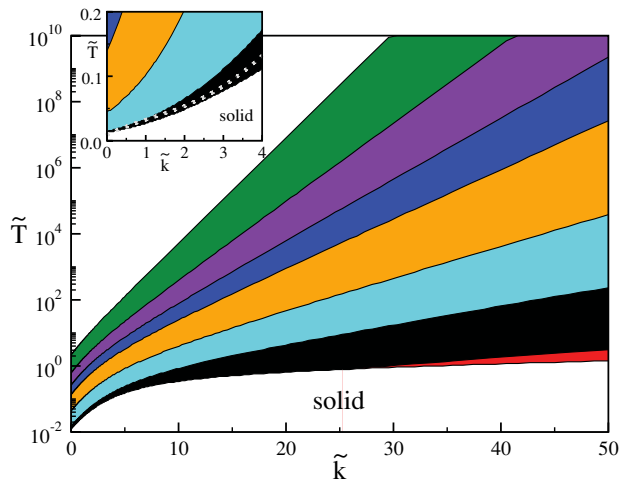
FIG. 12. Fluid-phase diagram, obtained using the MPB-RMSA, for HSY systems with $g_{\text{MPB-RMSA}}(\sigma^+) = 0$, fully characterized by the reduced temperature $\tilde{T}$ and screening parameter $\tilde{k}$. The fluid phase is characterized using the Hansen-Verlet criterion $S(q_m) < 3.2$. A specifically colored areal facet corresponds to a specific volume fraction, namely (from top to bottom) green: $\phi = 1\%$, violet: $\phi = 5\%$, blue: $\phi = 10\%$, orange: $\phi = 15\%$, light blue: $\phi = 25\%$, black: $\phi = 35\%$, and red: $\phi = 45\%$. A facet of given ϕ is bounded from above by the visible curve determined from $g(\sigma^+, \phi) = 0$, and from below by the freezing line $S(q_m) = 3.2$ common to all facets. Inset: lower-$\tilde{k}$ phase diagram part using a linear scale. The dotted curve is the solid-liquid coexistence line for point Yukawa particles according to Refs. 72 and 74.

solid from the fluid. However, it is overlaid in the figure by the differently colored areas of higher volume fractions. Increasing the temperature $\tilde{T}$ in systems of given ϕ and $\tilde{k}$ increases the likelihood of near-contact configurations, until the upper boundary of the fixed-ϕ segment is reached defined by the largest $\tilde{T}$ where $g_{\text{MPB-RMSA}}(\sigma^+) = 0$. On further increasing the temperature, $g(\sigma^+) > 0$ and the systems of a given ϕ no longer belong to the considered class of HSY systems with masked hard-core interactions. As expected and noted from the phase diagram, the region of fluid-state points describing systems with masked hard-core interactions narrows with decreasing screening length and increasing volume fraction.

According to the inset in Fig. 12, the solid-fluid coexistence line bounding the fluid-state diagram from below, is in good accord with the polynomial fit to the melting line,[72]

$$\tilde{T}_m(\tilde{k}) = 0.009 + 0.0303\tilde{k} - 0.00997\tilde{k}^2$$
$$+ 0.0035\tilde{k}^3 - 0.000245\tilde{k}^4, \quad (25)$$

reported by Bitzer *et al.*[74] The Hansen-Verlet criterion does not allow to distinguish the fluid-bcc transition appearing at smaller screening parameters from the fluid-fcc transition at larger $\tilde{k}$. However, the value of the reduced temperature at the isochoric fluid-bcc transition point in the OCP limit, is predicted by the MPB-RMSA method as $\tilde{T}(\tilde{k} = 0) \approx 0.01$. This value is in agreement with Eq. (25), and with the molecular dynamics simulation result by Hamaguchi et al.[38] This points to the internal consistency and accuracy of the fluid-phase diagram in Fig. 12. Note here that the fluid-solid coexistence region of the HSY at smaller values of $\tilde{k}$ is very narrow, with vanishing relative density difference (vanishing miscibility gap) at $\tilde{k} = 0$.[35,38,73]

A short discussion is in order here regarding the number of considered state points on which Fig. 12 is based. For each of the seven considered volume fractions, the MPB-RMSA pair structure functions have been calculated and stored in a database for 500×500 state points $(\tilde{T}, \tilde{k})$, of values distributed over the depicted $\tilde{T}$ and $\tilde{k}$ intervals. Such an extensive calculation was done in about 5 h of cpu time on a standard desktop PC. It was made possible owing to the rapidity and stability of the MPB-RMSA code. Out of this large number, systems with $S(q_m) < 3.2$ and $g_{\text{MPB-RMSA}}(\sigma^+) = 0$ were selected constituting the state points in Fig. 12. An additional filtering for systems obeying geometric concentration scaling has led to Fig. 11.

In Fig. 13, we have sorted the zero-contact-value systems in Fig. 12 according to values of the principal peak positions and locations, and the location, r_{dip}, of the first minimum in $g(r)$ to the right of the principal peak [see inset in Fig. 13(c)]. Each colored dot in the figure represents a system where the MPB-RMSA structure functions have been calculated. The subset of systems of lowest $\phi = 0.01$ (green dots), e.g., extends actually over the whole dotted phase space part. However, like in Fig. 12, it is partially overlayed [in Fig. 13(a) nearly completely] by the more concentrated subsets of systems colored like in Fig. 12.

Figure 13(a) shows explicitly that for a given value of $S(q_m)$, there exist a variety of systems of different peak values $g(r_m)$ and different volume fractions. As we have discussed in relation to Fig. 11 and the Hansen-Verlet criterion for $S(q_m)$, there is no unique value of $g(r_m)$ characterizing the onset of freezing. For instance, for $S(q_m) = 3.2$, values for $g(r_m)$ occur in between 2.2 and 3.8.

Figure 13(b) extends the discussion of Fig. 10 by showing that, with increasing ϕ, all systems approach geometric scaling behavior where $r_m/\tilde{d} = 1$ and $q_m\tilde{d}/(2\pi) = 1.1$. The most concentrated systems at $\phi = 0.45$ (in red) cover only a tiny patch centered at this geometric scaling point.

In Fig. 13(c), all fluid systems are sorted according to the locations, r_m and r_{dip}, of the principal peak and the subsequent minimum of $g(r)$. There is very roughly a linear relationship between r_{dip} and r_m (with some significant spread, however) independent of the considered volume fraction. Quite interestingly, the systems obeying geometric concentration scaling are located, for any considered ϕ, in a small patch centered at $r_{\text{dip}}/\tilde{d} = 1.4$ and $r_m/\tilde{d} = 1$, with constant ratio $r_{\text{dip}}/r_m \approx 1.4$ (as long as the fluid systems are well structured).

This finding of a constant ratio for systems obeying geometrical density scaling can be motivated by the following simplifying consideration. The rdf of a strongly correlated HSY system with well-developed principal peak is crudely described by

$$g(r) \approx \Theta(r - r_m) + \frac{A}{4\pi n r_m^2} \delta(r - r_m), \quad (26)$$

where $\Theta(r)$ is the unit step function. The δ-distribution part is a crude sketch of the peak region of $g(r)$. On noting that

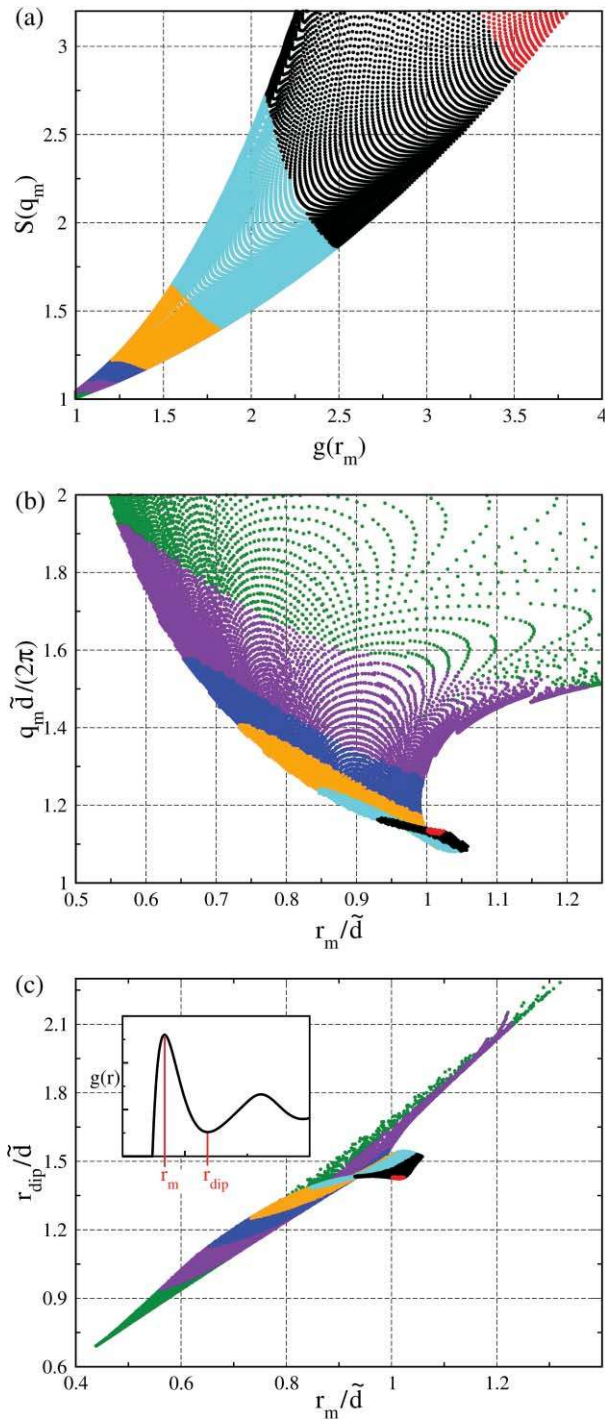$$N_{\text{nn}} = 4\pi n \int_0^{r_{\text{dip}}} dr\, r^2 g(r) \quad (27)$$

FIG. 13. (a) $S(q_m)$ vs $g(r_m)$, and (b) $q_m/(2\pi)$ vs $r_m/\tilde{d}$, and (c) r_{dip} vs r_m, for the zero-contact value fluid systems at the seven volume fractions considered in Fig. 12, using the same color code. All lengths are in units of $\tilde{d}$. Each colored dot represents a considered system. The inset in (c) illustrates the locations of r_m and r_{dip}.

defines the number of next neighbors, and using $r_m = \tilde{d}$, integration of Eq. (26) leads to

$$\left(\frac{r_{\text{dip}}}{r_m}\right)^3 = \frac{3}{4\pi}(N_{\text{nn}} - A) + 1. \qquad (28)$$

Provided A and N_{nn} are independent of ϕ, a constant ratio r_{dip}/r_m is obtained. In strongly correlated systems, $S(0) \approx 0$,

which in conjunction with the Fourier transform of Eq. (26) leads to $A = 4\pi/3 - 1$. Assuming $N_{\text{nn}} = 12$ consistent with the values $12-13$ obtained from Eq. (27) when the MPB-RMSA rdf's are used, $r_{\text{dip}}/r_m \approx 1.38$ is obtained which somewhat fortuitously is close to the ratio 1.4 noted from Fig. 13(c).

V. CONCLUSIONS

We have presented a comprehensive study of the static pair structure in liquids of particles with hard-sphere plus repulsive Yukawa pair interactions. The study comprises results from various integral equation schemes and MC simulations, and static light scattering results obtained from a well-characterized system of charged silica spheres.

An analytic integral equation method has been described which allows for a fast and quantitatively accurate computation of $S(q)$ and $g(r)$. The MPB-RMSA method is a slight modification of the PB-RMSA scheme originally devised by Snook and Hayter. It can be easily implemented into a standard (R)MSA code (cf., the Appendix), making it appealing for practical applications.

Through extensive comparison with RY and MC calculations, we have established the MPB-RMSA as a fast and convenient tool for analyzing experimental scattering data on charge-stabilized suspensions in a wide range of concentrations, ionic strengths, and effective charge numbers, with a fast delivery of $S(q)$ and $g(r)$. Such a fast delivery is also required in dynamic methods including the mode-coupling theory (MCT) and dynamic density functional theory, where numerous static structure factors in an extended range of wavenumbers are used as input in calculations of nonequilibrium boundaries such as the glass line.

The MPB-RMSA is well suited for the real-time fitting of experimentally obtained pair structure functions. The central fitting parameter, Z, can be obtained from matching the experimental structure factor peak heights. In most cases, the so-obtained MPB-RMSA effective charge number is practically identical to those obtained from the more elaborate MC simulation and RY methods. The latter two methods are computationally more expensive by orders of magnitude. For the charged silica spheres system studied experimentally, the effective charge predictions by the unmodified PB-RMSA scheme were found to be less accurate than the MPB-RMSA predictions.

We have demonstrated the capability of the MPB-RMSA as a fast tool for exploring generic features in the pair microstructure and the fluid phase behavior. Using the MPB-RMSA, the principal peak heights, $S(q_m)$ and $g(r_m)$, and the corresponding peak positions have been determined throughout the fluid-state $(\tilde{T}, \tilde{k})$ phase regime. This has allowed us to explore the conditions for which geometric concentration scaling of the peak positions is observed. The solid-fluid coexistence line determined in conjunction with the Hansen-Verlet freezing rule was shown to be in good agreement with MD simulation results for point Yukawa particles, including the OCP transition point.

While the MPB-RMSA static structure functions are in good overall agreement with the MC and RY results, in

some details there are smaller deviations. For low-salt systems of strongly correlated particles, $S(q_m)$ can be overestimated by up to 5%. Regarding the radial distribution function, the peak value, $g(r_m)$, is in general slightly underestimated, again by up to 5% for highly correlated particles. Furthermore, the (M)PB-RMSA $g(r)$ has a kink at the inflated (rescaled) hard core diameter not shared by the exact rdf. For HSY systems with weak Yukawa repulsion where the physical hard core matters, the MPB-MSA pair structure functions are also in good overall agreement with the MC and RY data, unless $\gamma e^{-k} \gtrsim 3.0$. Under the latter condition, the increase of $g(\sigma^+)$ as a function of ϕ is overestimated.

Unlike the RY scheme, the MPB-RMSA is thermodynamically inconsistent, but to a lesser degree than the RMSA, HNC and also the PB-RMSA schemes. The zero-q limit of $S(q)$ is predicted by the MPB-RMSA to reasonable accuracy, with deviations from the RY result of less than 10% even up to the freezing volume fraction.

Finally, we note that MPB-RMSA calculated pair structure functions have been used very recently as input in calculations of short-time diffusion properties of charge-stabilized colloidal spheres,[15,16] and in idealized MCT calculations of the colloidal glass transition.[75]

ACKNOWLEDGMENTS

APPENDIX: MPB-RMSA ALGORITHM

Here, we describe the algorithm of our MPB-RMSA code based on the analytic MSA solution for $S(q)$, $c(r)$, and the contact value $g(\sigma^+)$ of the HSY model as given in Refs. 43 and 44.

- Step 1:
  ```
  Specify input parameters [σ,γ,k,φ]
  of the considered repulsive HSY
  system. For charged colloids one may
  use Eqs. (2) and (3) for γ and k.
  Select tolerance 1≫TOL> 0 in Gillan
  criterion |g(x′ = 1⁺)| <TOL.
  ```
- Step 2:
  ```
  Calculate γ* = γ(1−φ)⁻², k_mod = (1−φ)k.
  ```
- Step 3:
  ```
  Determine g_MSA(x = 1⁺), with x = r/σ,
  using parameters [σ,γ*,k_mod,φ].
  If g_MSA(x = 1⁺) < 0, select s from (0,1)
  and continue with step 4.
  Otherwise assign σ* = σ, k* = k_mod,
  φ* = φ, then go to step 6
  ```

- Step 4:
  ```
  Assign x′ = xs, and:
  σ* = σ′ = σs⁻¹,
  φ* = φ′ = φs⁻³,
  γ* = γ′(1 − φ′)⁻² = γs(1 − φ′)⁻²,
  k′ = k_mod s⁻¹,
  k* = k′ − 2φ′¹ᐟ³ log(1 − φ′).
  ```
- Step 5:
  ```
  Determine g_MSA(x′ = 1⁺) for input
  parameters [σ*,γ*,k*,φ*].
  If |g_MSA(x′ = 1⁺)| <TOL, go to step 6.
  Otherwise select s from (0,1) and go
  to step 4.
  The new selection for s is made by
  a Newton-Raphson type algorithm, on
  accounting for previously obtained
  MSA contact values.
  ```
- Step 6:
  ```
  Calculate S_MSA(q) in given range
  0 ≤ q ≤ q_max using input parameters
  [σ*,γ*,k*,φ*], i.e. S_MPB−RMSA(q) =
  S_MSA(q;σ*,γ*,k*,φ*). The rdf fol-
  lows numerically by a fast Fourier
  transform.
  ```

If step 2 is replaced by $\gamma^* = \gamma(1 - \phi)^{-2}$ and $k_{\rm mod} = k$, the original PB-RMSA scheme by Snook and Hayter[52] is recovered. To obtain the rdf in MPB-RMSA, do not use Eq. (7) since the integrand decays slowly in q, making the integral quite sensitive to the cutoff wavenumber q_{max}. Instead, we use

$$g(r) = 1 + c(r) + \frac{1}{2\pi^2 r} \int_0^\infty dq\, q\, \sin(qr) \frac{(S(q) - 1)^2}{S(q)},$$
(A1)

which includes a faster decaying integrand. On the right-hand side of Eq. (A1), $S(q) = S_{\rm MPB\text{-}RMSA}(q)$ and $c(r > \sigma^*) = -\beta u^*(r)$, where $u^*(r) = u(r;\sigma^*,\gamma^*,k^*,\phi^*)$ and σ^* is the MPB-RMSA rescaled diameter. The MPB-RMSA code with TOL$= 10^{-4}$ requires in general less than 10 iterations to determine the rescaling parameter s. The execution time on a standard PC is less than 0.1 seconds, for $S(q)$ and $g(r)$ determined on a grid with 10^4 points.

[1] R. G. Palmer and J. D. Weeks, J. Chem. Phys. **58**, 4171 (1973).
[2] *Strongly Coupled Plasma Physics*, edited by S. Ichimuru (North Holland/Yamada Foundation, Amsterdam, 1990).
[3] J.-P. Hansen and I. R. McDonald, *Theory of Simple Liquids*, 2nd ed. (Academic Press, London, 1986).
[4] J. B. Hayter, R. Pynn, and J.-B. Suck, J. Phys. F **13**, F1 (1983).
[5] J. N. Herrera, P. T. Cummings, and H. Ruiz-Estrada, Mol. Phys. **96**, 835 (1999).
[6] A. J. Banchio, J. Bergenholtz, and G. Nägele, Phys. Rev. Lett. **82**, 1792 (1999).
[7] W. Härtl, J. Wagner, C. Beck, F. Gierschner, and R. Hempelmann, J. Phys.: Condens. Matter **12**, A287 (2000).
[8] Ch. Beck, W. Härtl, and J. Wagner, J. Chem. Phys. **111**, 8209 (2000).
[9] D. O. Riese, G. H. Wegdam, W. L. Vos, R. Sprik, D. Fenistein, J. H. H. Bongaerts, and G. Grübel, Phys. Rev. Lett. **85**, 5460 (2000).
[10] L. F. Rojas, C. Urban, P. Schurtenberger, T. Gisler, and H. H. von Grünberg, Europhys. Lett. **60**, 802 (2002).

[11]S. Zhou and X. Zhang, J. Phys. Chem. B **107**, 5294 (2003).
[12]A. J. Banchio, J. Gapinski, A. Patkowski, W. Häussler, A. Fluerasu, S. Saccana, P. Holmqvist, G. Meier, M. P. Lettinga, and G. Nägele, Phys. Rev. Lett. **96**, 138303 (2006).
[13]A. J. Banchio and G. Nägele, J. Chem. Phys. **128**, 104903 (2008).
[14]L. F. Rojas, C. Urban, R. Castaneda-Priego, V. Lobaskin, A. Stradner, F. Scheffold, and P. Schurtenberger, Phys. Rev. Lett. **100**, 178304 (2008).
[15]P. Holmqvist and G. Nägele, Phys. Rev. Lett. **104**, 058301 (2010).
[16]M. Heinen, P. Holmqvist, A. J. Banchio, and G. Nägele, J. Appl. Cryst. **43**, 970 (2010).
[17]J. Gapinski, A. Patkowski, A. J. Banchio, P. Holmqvist, G. Meier, M. P. Lettinga, and G. Nägele, J. Chem. Phys. **126**, 104905 (2007).
[18]J. Gapinski, A. Wilk, A. Patkowski, W. Häussler, A. J. Banchio, R. Pecora, and G. Nägele, J. Chem. Phys. **123**, 1054708 (2005).
[19]F. Zhang, M. W. A. Skoda, R. M. J. Jacobs, R. A. Martin, C. M. Martin, and F. Schreiber, J. Phys. Chem. B **111**, 251 (2007).
[20]G. Nägele, R. Klein, and M. Medina-Noyola, J. Chem. Phys. **83**, 2560 (1985).
[21]G. Senatore and L. Blum, J. Chem. Phys. **89**, 2676 (1985).
[22]M. G. McPhie and G. Nägele, Phys. Rev. E **78**, 060401(R) (2008).
[23]E. J. W. Verwey and J. Th. G. Overbeek, *Theory of the Stability of Lyophobic Colloids* (Elsevier, New York, 1948).
[24]M. Medina-Noyola and D. A. McQuarrie, J. Chem. Phys. **73**, 6279 (1980).
[25]L. Belloni, J. Chem. Phys. **85**, 519 (1986).
[26]H. Ruiz-Estrada, M. Medina-Noyola, and G. Nägele, Physica A **168**, 919 (1990).
[27]E. Trizac, L. Bocquet, M. Aubouy, and H. H. von Grünberg, Langmuir **19**, 4027 (2003).
[28]A. Torres, G. Tellez, and R. van Roij, J. Chem. Phys. **128**, 154906 (2008).
[29]S. Pianegonda, E. Trizac, and Y. Levin, J. Chem. Phys. **126**, 014702 (2007).
[30]T. E. Colla, Y. Levin, and E. Trizac, J. Chem. Phys. **131**, 074115 (2009).
[31]A. P. dos Santos, A. Diehl, and Y. Levin, J. Chem. Phys. **123**, 104105 (2010).
[32]W. B. Russel and D. W. Benzing, J. Colloid Interface Sci. **83**, 163 (1981).
[33]A. R. Denton, Phys. Rev. E **62**, 3855 (2000).
[34]A.-P. Hynninen and M. Dijkstra, J. Phys.: Condens. Matter **15**, S3557 (2003).
[35]E. J. Meijer and D. Frenkel, J. Chem. Phys. **94**, 2269 (1991).
[36]M. J. Stevens and M. O. Robbins, J. Chem. Phys. **98**, 2319 (1993).
[37]N. Pistoor and K. Kremer, Physica A **201**, 171 (1993).
[38]S. Hamaguchi, J. Chem. Phys. **105**, 7641 (1996); *ibid*.Phys. Rev. E **56**, 4671 (1997).
[39]J. M. Brader, Int. J. Thermophys. **27**, 394 (2006).
[40]F. E. Azhar, M. Baus, J.-P. Ryckaert, and E. J. Meijer, J. Chem. Phys. **112**, 5121 (2000).
[41]E. Waisman, Molec. Phys. **25**, 45 (1973).
[42]J. S. Hoye and L. Blum, J. Stat. Phys. **19**, 317 (1978).
[43]P. T. Cummings and E. R. Smith, Mol. Phys. **38**, 997 (1979).
[44]P. T. Cummings and E. R. Smith, J. Chem. Phys. **42**, 241 (1979).
[45]M. Ginoza, J. Phys. Soc. Japan **55**, 95 (1986).
[46]J.-P. Hansen and J. B. Hayter, Mol. Phys. **46**, 651 (1982).
[47]M. J. Gillan, J. Phys. C **7**, L1 (1974).
[48]SANS Manuals and Data Reduction, http://www.ncnr.nist.gov/programs/sans/data/index.html.
[49]J. Gapinski, A. Patkowski, and G. Nägele, J. Chem. Phys. **132**, 054510 (2010).
[50]S. K. Lai and G. F. Wang, Phys. Rev. E **98**, 3072 (1998).
[51]F. J. Rogers and D. A. Young, Phys. Rev. A **30**, 999 (1984).
[52]I. K. Snook and J. B. Hayter, Langmuir **8**, 2880 (1992).
[53]R. J. Hunter, *Foundations of Colloid Science*, 2nd ed. (Oxford University Press, Oxford, 2001), Chap. 14.
[54]G. Nägele, M. Medina-Noyola, and R. Klein, Physica A **149**, 123 (1988).
[55]J. B. Hayter and J. Penfold, Mol. Phys. **42**, 109 (1980).
[56]S. K. Lai, G. F. Wang, W. P. Peng, and J. L. Wang, Physica B **269**, 183 (1999).
[57]B. Svensson and B. Jönsson, Mol. Phys. **50**, 489 (1983).
[58]B. Beresford-Smith, D. Y. C. Chan, and D. J. Mitchell, J. Colloid Interface Sci. **105**, 216 (1984).
[59]S. Khan, T. L. Morton, and D. Ronis, Phys. Rev. A **35**, 4295 (1987).
[60]L. Belloni, J. Phys.: Condens. Matter **12**, R549 (2000).
[61]T. Morita, Prog. Theo. Phys. **20**, 920 (1958).
[62]A. A. Louis, Phil. Trans. R. Soc. Lond. A **359**, 939 (2001).
[63]A. A. Louis, J. Phys.: Condens. Matter **14**, 9187 (2002).
[64]M. Dijkstra, R. van Roij, and R. Evans, J. Chem. Phys. **113**, 4799 (2000).
[65]J. Dobnikar, R. Castaneda-Priego, H. H. von Grünberg, and E. Trizac, New J. of Phys. **8**, 277 (2006).
[66]E. Trizac, L. Belloni, J. Dobnikar, H. H. von Grünberg, and R. Castaneda-Priego, Phys. Rev. E **75**, 011401 (2007).
[67]F. H. Stillinger, H. Sakai, and S. Torquato, J. Chem. Phys. **117**, 288 (2002).
[68]C. F. Tejero and M. Baus, J. Chem. Phys. **118**, 892 (2003).
[69]C. F. Tejero, J. Phys.: Condens. Matter **15**, S395 (2003).
[70]A. P. Philipse and A. Vrij, J. Chem. Phys. **88**, 6459 (1988).
[71]J.-P. Hansen and L. Verlet, Phys. Rev. **184**, 151 (1969).
[72]K. Kremer, M. O. Robbins, and G. S. Grest, Phys. Rev. Lett. **57**, 2694 (1986).
[73]D. C. Wang and A. P. Gast, J. Phys.: Condens. Matter **11**, 10133 (1999).
[74]F. Bitzer, T. Palberg, H. Löwen, R. Simon, and P. Leiderer, Phys. Rev. E **50**, 2821 (1994).
[75]H. Kaiser, M. Heinen, G. Nägele, G. Maret, and M. Fuchs (in preparation).